Chapter 4

Relevance of electrochemically synthesized AuNP decorated GO functionalized PEDOT- PSS based electrodes for electrochemical sensing of Glucose and Aflatoxin B_1

This chapter outlines on reliable, field usable, versatile and direct electrochemical sensors based on conducting polymer composite electrode, Poly (3,4-ethylenedioxythiophene): polystyrene sulphonic acid (PEDOT-PSS) and graphene oxide (GO) decorated with spherical gold nanoparticles (AuNPs), for glucose sensing and label-free detection of AF-B_1. To demonstrate biosensing advantages of these electrodes, interaction between covalently immobilized glucose oxidase (*GlOx*) enzyme and D-glucose is monitored via chronoamperometry and cyclic voltammetry (CV). Validation of the glucose sensors has shown satisfactory results using real saliva samples. Two different electroanalytical techniques namely, transient capacitance and differential pulse voltammetry (DPV) has been compared, to select the most prominent technique for analyzing the mycotoxin easily. For demonstration of application of this sensor directly using minimum sample preparation, AF-B_1 sensing has been confirmed successfully using white button mushrooms and okra stored at ambient conditions.

4.1. Introduction

In recent years, diabetes mellitus (DM) has become one of the most prevalent chronic diseases for life throughout the world [1]. It is estimated that, approximately 537 million people worldwide are suffering from diabetes, with a total of several million people dying every year as a result of this disease [2,3]. In a variety of fields ranging from biomedical applications to ecological approaches, glucose detection and monitoring is of prime interest [4]. A high glucose level continues to persist in diabetic patients as a result of the inability to regulate the sugar level in the blood causing diabetic ketoacidosis [5-7]. There are a number of serious complications associated with long-term hyperglycemia, including chronic lesions to the kidneys, eyes, heart, and nerves, resulting in reduced quality of life and increased mortality worldwide [5,7,8,9]. Moreover, hypoglycemia, which is caused due to lower blood glucose level leads to multiple organ failure, Cardiac arrhythmias, brain damage etc. In order to reduce or prevent these complications rapid, accurate, fast, cost-effective glucose sensors with long lifetime stability and sensitivity are important for monitoring requirement.

Again, low molecular weight (MW=0.7 kD) mycotoxins are produced by filamentous fungi occurring in food, feedstuffs and other raw materials which cause illness leading to death of animals and humans [10-14]. Among mycotoxins family Aflatoxin B_1 (AF-B_1) is the most dangerous one, produced by a variety of *Aspergillus* species [15,16]. AF-B_1 is considered as the most hepatotoxic and hepatocarcinogenic classified as a group 1A carcinogen to humans [17] and they are found in many crops like pistachios, spices, peanuts, corn, Brazil nuts, copra, cottonseed etc [11,18]. Permissible limit of AF-B_1 in nuts and cereals is 5 µg/kg in milk and milk products (AF-M_1), it is ~500 pg/mL. Therefore, the development of a fast, cost-effective, portable, ready-to-use platform can be a point-of-care (POC) solution for precise monitoring of AF-B_1 with high sensitivity and selectivity.

Prior to therapeutics, role of diagnostic tests in medical care is very important. Usually, most of the requisite tests performed are laboratory based immunoassays such as thin-layer chromatography, liquid chromatography mass spectrometry, enzyme linked immunosorbent assay (ELISA), high performance liquid chromatography etc. which are expensive, time-consuming and require trained personnel for the experiment. To address these limitations while making tests simple and user-friendly, development of advanced biosensors with faster measurement times and lower costs is very crucial. Electrochemical detection technique is one of the most popular ones due to its simplicity, high sensitivity, portability, good analytical performances and low costs [19]. Due to these advantages electrochemical sensors are suitable for POC applications, for routine health check-ups including monitoring and testing toxicity aspects [20,21]. Various nanostructured materials and composites are being explored for cost effective and reliable electrochemical biosensors, however, commercialization is still lacking.

The unique properties of conducting polymers make them deployable in applications such as, supercapacitors, solar cells, biosensors, and flexible electronics [22]. Amongst many flexible conducting polymers, PEDOT-PSS has been identified as a suitable candidate for biosensing because of its enhanced electrical conductivity, mechanical flexibility, chemical stability and existence of suitable functional groups in the backbone of the polymer which can attach biomolecules [23,24]. Graphene oxide (GO), one of the widely investigated 2D materials, comes with plentiful oxygen functional

groups like epoxides, hydroxyl, carboxyl etc. which could make it hydrophilic in nature and dispersible in aqueous solutions. Furthermore, presence of these functional moieties helps in immobilization of biomolecules through covalent linkages [25-27] making it suitable for a reliable biosensor electrode with PEDOT-PSS. Presence of Au nanoparticles (AuNP) layers over polymer-GO composite provides better charge transport mechanism between the electrode-electrolyte interface and enhances the conductivity of the system [28].

In this chapter, we demonstrate the versatility of solution processible, AuNPs/GO/PEDOT-PSS electrode for electrochemical glucose sensing and AF-B_1 sensing with better sensitivity, cost effectiveness and repeatability.

(A) Glucose sensor

4.2. Electrochemical studies of the Glucose biosensors

To understand the interfacial charge transfer kinetics after every process step of sensor fabrication, cyclic voltammetry was performed for all the prepared PEDOT-PSS, GO/PEDOT-PSS, AuNP/GO/PEDOT-PSS at a scan rate of 20 mV/s under the potential window from -0.2 V to 1.2 V [29,30] in 0.1 M PBS (phosphate buffer saline) as an electrolyte (pH 7.4). Multifrequency impedance spectroscopy study was carried out for the composite electrodes and the sensor after each process step with an ac signal of 10 mV within frequency range from 1 Hz to 1 MHz in PBS electrolyte (pH 7.4). The amperometric response of interaction between glucose and glucose oxidase was monitored via chronoamperometry.

4.2.1. Cyclic voltammetry (CV) studies of Glucose sensor

The electrochemical behaviour of PEDOT-PSS/ITO, GO/PEDOT-PSS/ITO and AuNP/GO/PEDOT-PSS/ITO electrodes after each step of processing i.e., before and after immobilization of enzyme glucose oxidase (*GlOx*) and after interaction with glucose has been analyzed by employing CV within the potential window of -0.2 V-1.2 V at a scan rate of 20 mV/s, as shown in Figure 4.1. The CV plots for the ITO electrode modified with PEDOT-PSS and GO functionalized PEDOT-PSS after glutaraldehyde adsorption, *GlOx* immobilization, glucose interaction are depicted in Figure 4.1 (a,b) respectively. In fact, for both cases the area under the CV curve decreases after glutaraldehyde uptake as well

as after enzyme immobilization treatment. This may be due to the lesser charge transfer process between the electrode and electrolyte interface with additional glutaraldehyde and enzyme layers. Both PEDOT-PSS and GO functionalized PEDOT-PSS electrodes showed increase in the current and capacitance after glucose interaction with the enzyme glucose oxidase. The CV plots for AuNP/GO/PEDOT-PSS/ITO electrode after every processing step can be found in Figure 4.1 (c). However, notable shifting in the positions of reduction peaks at 0.22 V was observed after each process steps for the Au functionalized composite electrode. Moreover, the broad reduction peak at 0.22 V for the AuNP/GO/PEDOT-PSS/ITO electrode in the PBS electrolyte gets shifted to 0.31 V with a reduced current of 367 μA after glutaraldehyde treatment. This cross-linking can change the electronic environment and alter the electrochemical properties of the material, resulting in shifts in the reduction peak. Upon enzymatic treatment of *GlOx*, the reduction peak shifted to 0.4 V while an additional oxidation peak emerges at ~ 0.7 V when treated with glucose solution. Nevertheless, after enzyme-glucose interaction the redox peak currents of the ternary electrode increases due to a better charge transfer process between the electrode-electrolyte interface resulting in an enhancement of the area under the CV curve. This is, because of the reaction of glucose with co-enzyme flavin adenine dinucleotide (FAD) in *GlOx* [31-33].

The electroactive enzyme cofactor FAD of *GlOx* undergoes a two-electron coupled with two-proton redox reaction as shown in equation (4.1). Furthermore, *GlOx* oxidizes glucose to D-glucono-1,5-lactone accompanied by transferring of two protons and two electrons from glucose to FAD and form $FADH_2$ eventually. Using FAD/ $FADH_2$ redox centres of *GlOx* [33-35], the reaction can be written as

$$GlOx\text{-}FADH_2 \rightarrow GlOx\text{-}FAD + 2H^+ + 2e^- \quad (4.1)$$

When glucose was added, the enzyme-catalyzed reaction between FAD and glucose produces an increase in the reduction peak current along with the oxidation peak at 0.7 V which can be explained in the following equations,

$$\text{Glucose} + GlOx\ (\text{FAD}) \rightarrow \text{Gluconolactone} + GlOx\ (FADH_2) \quad (4.2)$$

$$\text{GlOx}\ (FADH_2) + O_2 \rightarrow \text{GlOx}\ (\text{FAD}) + H_2O_2 \quad (4.2.1)$$

$$\text{i.e., } \beta\text{-D-glucose} + O_2 \rightarrow \text{D-glucono-1,5-lactone} + H_2O_2 \quad (4.2.2)$$

As glucose oxidase oxidizes β-D-glucose to D-gluconolactone and H_2O_2 resulting in change in electron concentration, change in the redox peak can be observed.

The redox peak current increases after glucose treatment and is ascribed to charge transfer process indicating successful reaction of glucose with *GlOx*. Accordingly, acquired CV responses of the fabricated *GlOx*/GLU/AuNP/GO/PEDOT-PSS/ITO electrode for different glucose concentrations can be found in the Figure 4.1 (d). The redox-peak current of the biosensor increases significantly after addition of 10, 15, 30, 50 and 100 µM glucose; respectively.

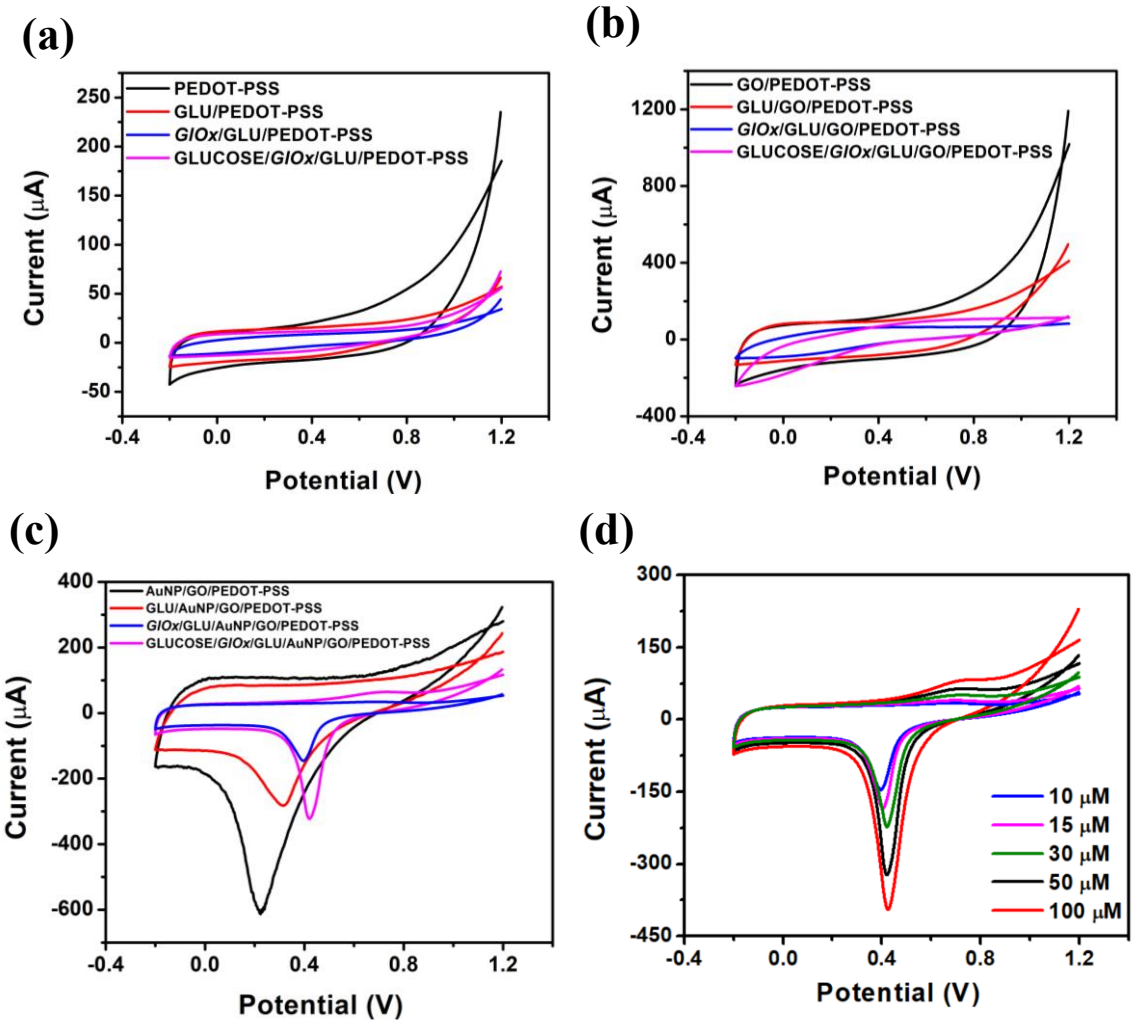

Figure 4.1: Cyclic voltammetry plots of (a) PEDOT-PSS/ITO sensor (with 10 µM glucose), (b) GO/PEDOT-PSS/ITO sensor after each process step, with final step of 13.62 µM glucose interaction, (c) AuNP/GO/PEDOT-PSS/ITO sensor after each process step and with addition of 347.72 µM glucose, (d) *Glox*/GLU/AuNP/GO/PEDOT-PSS bioelectrode at different glucose concentrations.

4.2.2. Electrochemical Impedance studies of Glucose sensor

The charge transfer kinetics between the as-prepared PEDOT-PSS/ITO, GO/PEDOT-PSS/ITO and AuNP/GO/PEDOT-PSS/ITO electrodes and the electrolyte interface have been characterized through EIS technique, performed within the frequency range, 1 Hz - 1 MHz with a small signal of ac typically10 mV. The impedance spectral responses of the fabricated working electrode with Ag/AgCl as reference electrode and platinum as counter electrode can be found in Figure 4.2.

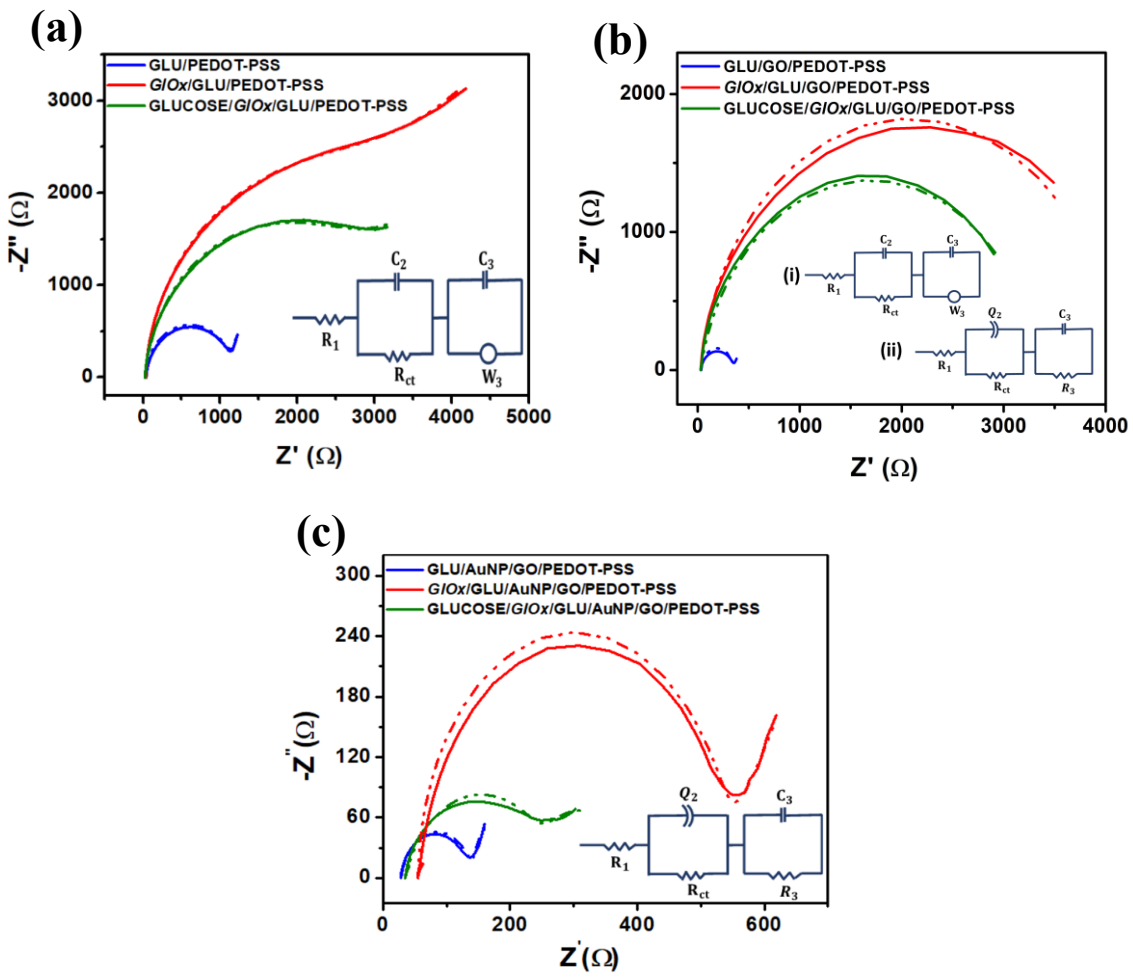

Figure 4.2: Impedance response of (a) PEDOT-PSS/ITO sensor (glucose concentration 10 µM), (b) GO/PEDOT-PSS/ITO sensor (with addition of glucose concentration 13.62 µM), (c) AuNP/GO/PEDOT-PSS/ITO sensor (with addition of glucose concentration 347.72 µM) after each process steps.

Impedance data were fitted with equivalent circuit which consists of: series resistance (R_1) in series with the parallel combination of charge transfer resistance (R_{ct}) and double layer capacitor (C_2) and another parallel combination of Warburg impedance (W_3) which represents the diffusion in the polymer chain with capacitor (C_3) representing the space charge layer amidst PEDOT and PSS rich grains.

The Nyquist plots of the respective PEDOT-PSS/ITO, GO/PEDOT-PSS/ITO and AuNP/GO/PEDOT-PSS/ITO electrodes after each process steps of glutaraldehyde treatment, enzyme immobilization and enzyme-glucose interaction can be found in Figure 4.2 (a-c). Distinctly different impedance spectra could be observed during the various processing steps of the electrodes under study. Total impedance of the electrode increases after *GlOx* immobilization and it drops substantially after glucose interaction for all the three types of electrodes. In fact, *GlOx* hinders the charge transfer between the probe and the electrolyte surface, tending to reduce the charge transfer events owing to its large molecular size resulting in enhanced impedance value. Here, the enzymes are covalently attached at the surface of the electrode through glutaraldehyde cross linker. The *GlOx* catalyses the glucose and would result in a better charge transfer event. Although CV plots for the corresponding electrodes showed an increase in current and capacitance after glucose interaction, both PEDOT-PSS and GO/PEDOT-PSS did not show significant changes whereas Au/GO/PEDOT-PSS offered observable changes both in CV and impedance plots. This suggests the usefulness of the tertiary electrode over other two electrodes for effective sensing purposes.

Even though slight increase in impedance is observed after various process steps for the Au/GO/PEDOT-PSS sensor, the impedance data fitted well with the same equivalent circuit. Warburg impedance converting into resistive impedance after *GlOx* immobilization is indicated in Figure 4.2 (a,b) by the absence of increased impedance in the low frequency region. Modified equivalent circuit is shown in the inset of Figure 4.2 (b). The corresponding changes in the circuit parameters employed for fitting the impedance data using the tertiary electrode after each process steps are depicted in Table 4.1. Charge transfer resistance, constant phase element and resistance between PEDOT and PSS grains increased with *GlOx* immobilization. Whereas, all the above three components declined after enzyme catalyzed reaction with glucose indicating excess charge carrier generation and space charge layer modification.

Table 4.1: Fitted parameters of EIS spectra for the ternary (AuNP/GO/PEDOT-PSS) electrode after every process step of sensor fabrication.

Serial number	Electrode	R_1 (Ω)	R_{ct} (Ω)	Q_2 ($\times 10^{-6}$) S.s^n	R_3 (Ω)	C_3 (μF)
1	GLU/AuNP/GO/ PEDOT-PSS	28.45	114	25.22, n= 0.855 Q_2^n =17.39	144	2407
2	*GlOx*/GLU/AuNP/GO/ PEDOT-PSS	54.93	482.3	1247, n= 0.779 Q_2^n =258.03	1055	3611
3	GLUCOSE/*GlOx*/GLU/ AuNP/GO/PEDOT-PSS	33.69	231.8	48.84, n= 0.764 Q_2^n =19.50	115	1127

4.3. Chronoamperometry studies of glucose sensor

Chronoamperometric method was employed for estimating the linear range of glucose detection by the as-fabricated bioelectrodes. The chronoamperometry behaviour for the PEDOT-PSS/ITO and GO/PEDOT-PSS/ITO electrodes are presented in Figure 4.3 (a,b). As can be found, the PEDOT-PSS/ITO electrode offers a poor linearity as seen from the current response to each addition of glucose. Noticeably, the selectivity of the sensor was better after GO incorporation but with lowered response towards oxidation of glucose. The *GlOx*/GLU/AuNP/GO/PEDOT-PSS/ITO electrode at different concentrations of glucose under the oxidation potential of 0.7 V with respect to (Ag/AgCl) electrode featuring dynamic nature of change as can be found in Figure 4.4 (a). At every step, different concentrations (100-1500) μM of glucose has been injected. The glucose sensor exhibited a noticeable change in current with increase in the concentration of glucose. The modified electrode showed a systematic increase in current with subsequent addition of glucose in each step (Figure 4.4 (a)). To check the selectivity of the fabricated sensor, 20 μL of ascorbic acid with concentration 1 mM was added at position A. After the addition of ascorbic acid, the response showed only a ripple in current indicating no significant changes, suggesting desired selectivity for the glucose sensor.

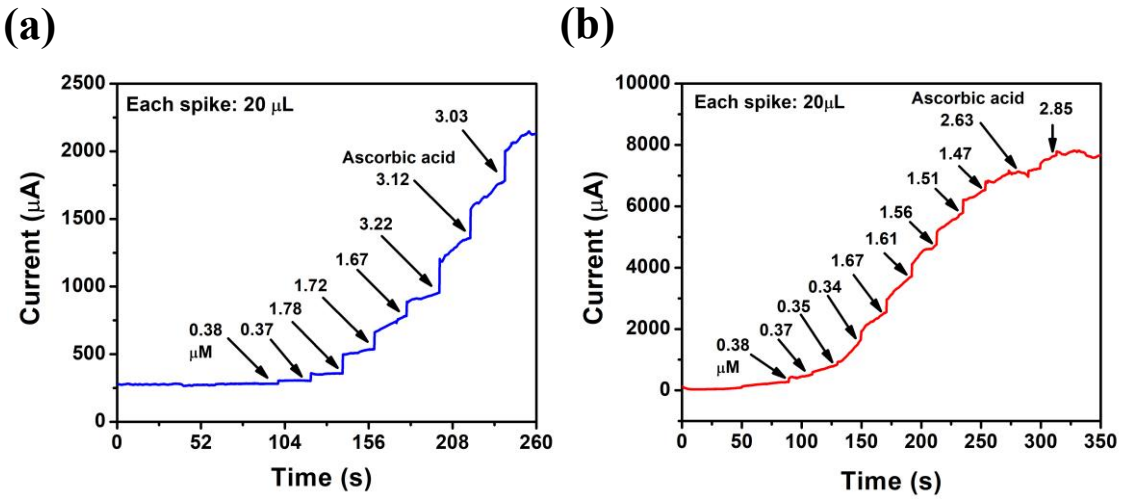

Figure 4.3: Chronoamperommetry plot of (a) PEDOT-PSS/ITO (b) GO/PEDOT-PSS/ITO electrodes at different glucose concentrations at a potential of 0.8 V.

Another selectivity test was conducted for the sensor in presence of multiple interference species, shown in Figure 4.4 (b). The selectivity test was performed with three common interfering compounds: ascorbic acid, sucrose and uric acid by taking same concentration of 1 mM each. Evidently, none of these species, except for glucose, had any influence on both electrodes suggesting very good selectivity. This demonstrates the outstanding anti-interference capability of both sensors, highlighting its high selectivity towards glucose.

However, the changes in current (ΔI) vs. concentration of the electrolyte (after each successive addition of glucose) for AuNP/GO/PEDOT-PSS bioelectrode showed linear fit in Figure 4.4 (c). By performing a linear fit, linear regression line was obtained and the sensitivity of the enzymatic sensor was estimated as, 10.59 µA μM^{-1} and LOD (= $3.3\times\sigma/m$, σ= standard deviation in y intercept, and m= slope of the regression line [36]) was 2.33 µM. Linear regression plot (R^2: 0.99) of Conc. (both µM and mg/dL) vs ΔI for AuNP/GO/PEDOT-PSS/ITO sensors is shown in Figure 4.4 (d) for comparison with clinical estimates of glucose. The developed AuNP/GO/PEDOT-PSS/ITO sensor showed a linearity within 0.069 mg/dL - 6.72 mg/dL.

Hence, AuNP/GO/PEDOT-PSS/ITO electrode has been a better candidate for sensing activity, selectivity while offering a wider linear range.

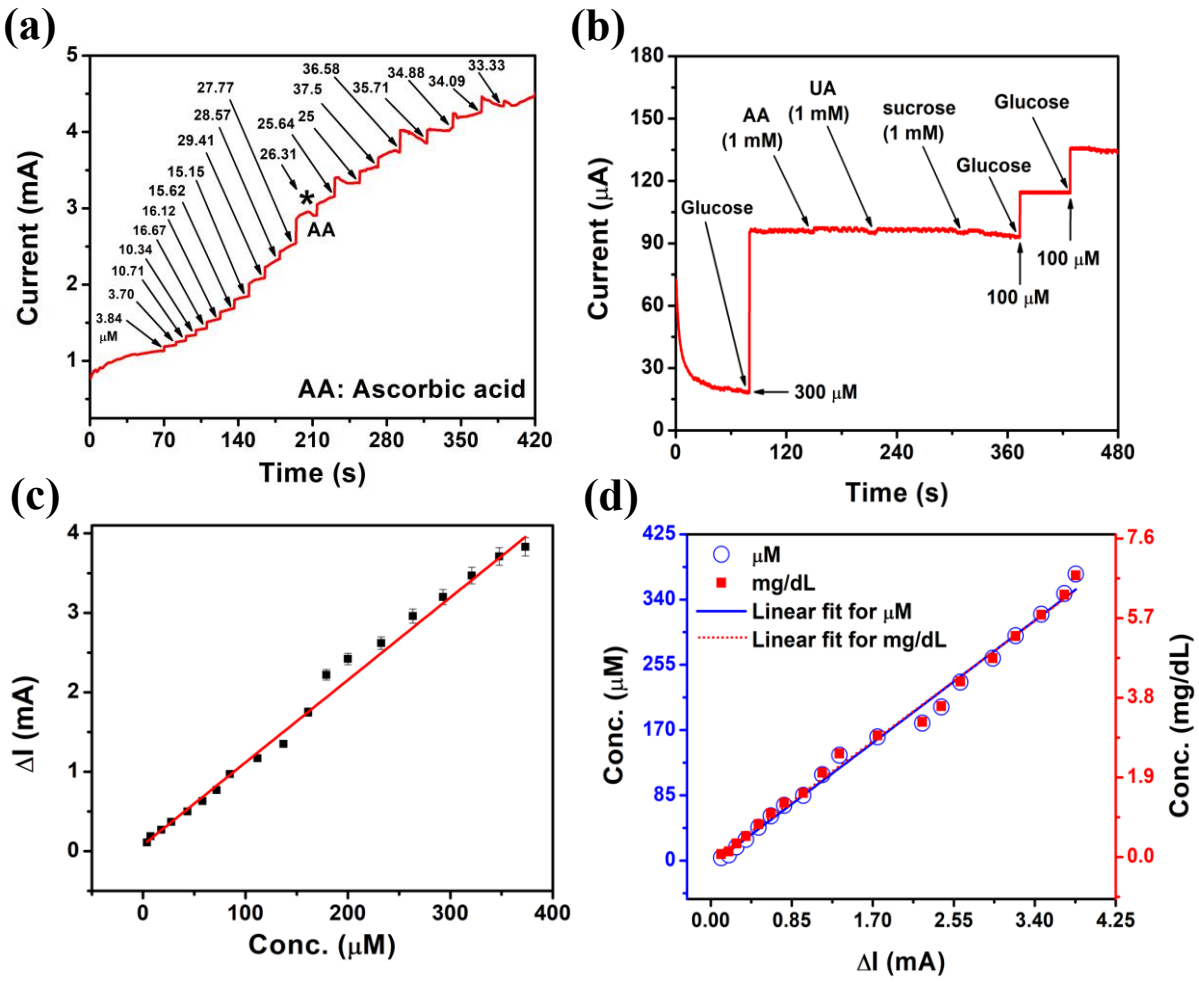

Figure 4.4: (a) Chronoamperometry plot of AuNP/GO/PEDOT-PSS/ITO electrode at different concentrations of glucose. (b) Selectivity test in presence of different interference like ascorbic acid (AA), uric acid (UA), sucrose (1 mM of each). (c) Linear regression plot of current vs. concentration for AuNP/GO/PEDOT-PSS/ITO biosensor with error bar. (d) Linear regression plot of Conc. (both μM and mg/dL) vs ΔI for AuNP/GO/PEDOT-PSS/ITO.

With an aim to develop a reliable amperometric glucose sensor, repeatability studies were performed and the results are enlisted in Table 4.2, which ensure good repeatability over a wide linear range of 3.84-320.93 μM and within an acceptable error of ±3%. Thus, the obtained LOD is comparable, or better than most of the reported conducting polymer based glucose sensors [37-41].

Table 4.2: Results of AuNPs embedded GO/PEDOT-PSS glucose sensor from repeatable experiment.

Serial Number	Electrode	LOD (μM)	Sensitivity (μA μM^{-1})	Linear range (μM)
1	AuNP/GO/PEDOT-PSS, sensor 1	13.44	10.59	3.84-373.33
2	AuNP/GO/PEDOT-PSS, sensor 2	3.64	13.98	3.84-347.72
3	AuNP/GO/PEDOT-PSS, sensor 3	13.51	10.34	3.84-232.5
4	AuNP/GO/PEDOT-PSS, sensor 4	8.60	6.84	3.84-320.93
5	AuNP/GO/PEDOT-PSS, sensor 5	14.06	7.32	3.84-263.41

4.4. Performance of glucose sensors towards real sample

The importance of sugar detection in real human biological samples at home, outside of clinical settings, is driven by several key factors like convenience, better health management, and technological advancements. The current techniques, such as finger-prick tests, often prevent regular monitoring since they are invasive and frequently uncomfortable. Finger pricking can cause temporary discomfort, bruising, fainting, and the risk of blood-borne infections. Therefore, a non-invasive and simple method for diagnosing and monitoring diabetes is highly desirable. Non-invasive glucose sensing devices that can deliver precise and reliable findings without the pain and inconvenience of blood testing are very crucial. Among all, detection of glucose in saliva is one of the most desirable non-invasive techniques. Notably, collecting saliva is easy and quick, making it suitable for frequent monitoring and use in various settings, including at home, work, or on the go etc. Saliva testing is an inexpensive and painless alternative to blood draws. To implement the glucose sensing in saliva sample, two volunteers were enrolled, one is non diabetic (sample 1) and another is diabatic (sample 2). The saliva sample was collected using cotton swabs from the two volunteers in the fasting condition (before having food). Each saliva swab was separately mixed with 0.1 M PBS, cotton was squeezed and the remaining solution was shaken well [42]. Afterwards, the saliva solutions were filtered individually to remove any contaminant and the filtrate was used for further experiment.

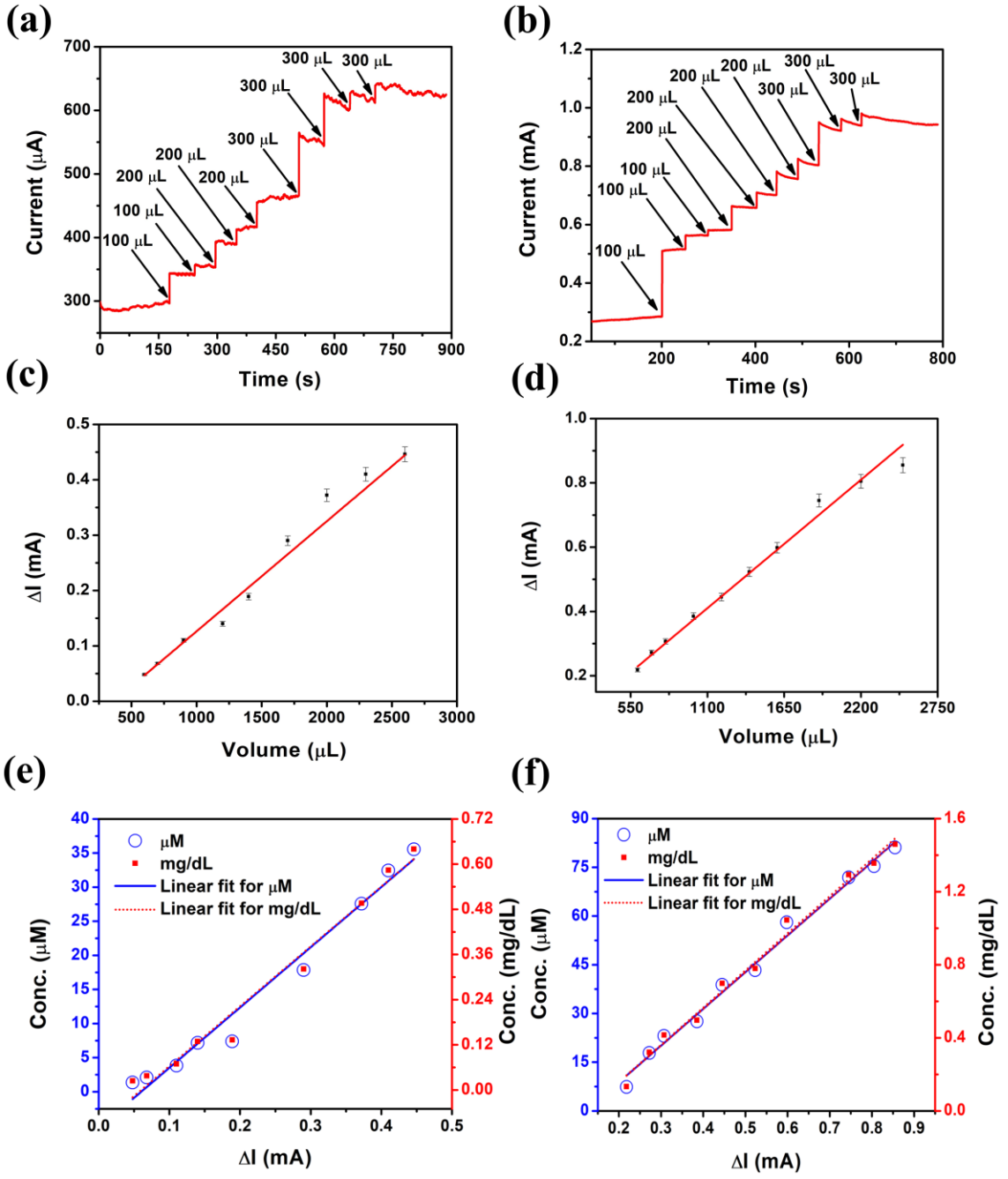

Figure 4.5: Chronoamperometry plots of AuNP/GO/PEDOT-PSS/ITO electrode at different volume of salivary sample (a) sample 1, (b) sample 2. Linear regression plot of current vs. volume for AuNP/GO/PEDOT-PSS/ITO electrode of (c) sample 1, (d) sample 2 with error bars. Linear regression plot of Conc. (both μM and mg/dL) vs ΔI (e) sample 1 and (f) sample 2.

Chronoamperometry technique was employed to perform glucose sensing in real samples with *Glox*/GLU/AuNP/GO/PEDOT-PSS/ITO, adding different volumes of samples at different time intervals. While performing Chronoamperometry, after obtaining a stable baseline different volumes of saliva solution was injected as a function of time. The chronoamperometry plot of AuNP/GO/PEDOT-PSS/ITO electrode for sample 1 and sample 2 is shown in Figure 4.5 (a) and (b); respectively. Repeatability has been performed for the sensor, where sample 1 showed 3% error and sample 2 showed 2.7% error, Figure 4.5 (c) and (d). Again, linear regression plot (R^2: 0.97) of conc. (both µM and mg/dL) vs ΔI for sample 1 and sample 2 is shown in Figure 4.5 (e, f); respectively. While comparing with standard glucose testing (Figure 4.4 (d)) sample 1 showed a maximum concentration of 35.56 µM (0.675 mg/dL) and sample 2 showed maximum of 81.82 µM (1.472 mg/dL) glucose presence.

(B) Aflatoxin B_1 sensor

4.5. Electrochemical studies of the AF-B_1 immunosensors

CV curves were recorded for the fabricated electrodes after every processing step of senor fabrication in presence of 0.1 M PBS as electrolyte at a scan rate, 20 mV/s within a potential range of -0.2 V-1.2 V [29,30]. Moreover, electrochemical impedance spectroscopy (EIS) was employed within a frequency window 1 Hz - 1 MHz, with 10 mV peak- to -peak ac voltage and 0 V dc bias. Here, AF-B_1 antigen detection was carried out by performing two techniques: transient capacitance measurements at 77 Hz and 1 kHz and differential pulse voltammetry (DPV).

4.5.1. Cyclic voltammetry studies of Aflatoxin B_1 sensor

The electrochemical behaviour of AuNP/GO/PEDOT-PSS/ITO electrode after each step of processing i.e., before and after immobilization of antibody and after interaction with antigen has been analysed by employing CV within the potential window of -0.2 V-1.2 V at a scan rate of 20 mV/s. For developing label-free AF-B_1 sensor using two electrochemical methods, we have cross verified the LOD for AF-B_1 using PBS, (**electrolyte 1**) and ferrocyanide/ferricyanide redox couple(electrolyte PBS+$[Fe(CN)_6]^{3-/4}$, **electrolyte 2**).

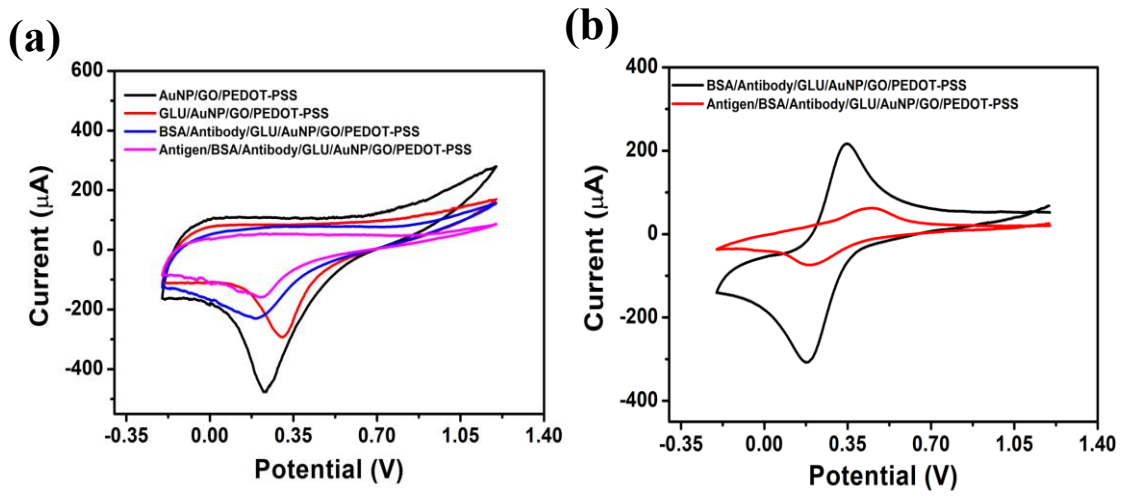

Figure 4.6: Cyclic voltammetry plot of anti-AF-B_1/AuNP/GO/PEDOT-PSS/ITO sensor within a potential window of -0.2 V to 1.2 V and at a scan rate of 20 mV/s in (a) PBS (electrolyte1) after each process step, with final step of injecting antigen concentration. (b) 100 mM PBS and 5 mM $[Fe(CN)_6]^{3-/4-}$ (electrolyte 2) after 594.59 ng mL^{-1} AF-B_1 addition.

The CV plots recorded for AuNP/GO/PEDOT-PSS with electrolyte 1 and 2 are shown in Figure 4.6 (a and b) respectively. As can be found in Figure 4.6 (b), the modified electrodes exhibited well defined redox peaks attributed to the electron transfer between solution $[Fe(CN)_6]^{3-/4-}$ and the electrode [Fe (III) ↔ Fe(II) + e'] [30]. Further, the area under the CV curves decreases after interaction of the anti-AF-B_1 with AF-B_1 due to slow charge transfer between the electrode and electrolyte interface primarily due to immunocomplex formation. Even in the absence of redox couple there is a systematic decrease in the reduction peak current with peak shift (Figure 4.6 (a)) which can be used for monitoring immunocomplex formation. The reduction peak detected at 0.22 V gets shifted to 0.30 V with reduced current on glutaraldehyde treatment. Whereas, the immobilization of antibody leads to shifting of the reduction peak with reduced current due to the fact that, the antibody hinders the transfer of charges at the electrode-electrolyte interface. After interaction of analyte with the antibody the area under the curve is drastically reduced along with reduction peak current which indicates relatively less charge transfer between the electrode and electrolyte interface suggesting better sensitivity with capacitive measurements.

4.5.2. Electrochemical Impedance Studies of Aflatoxin B_1 sensor

The charge transfer kinetics after every step of sensor fabrication between the as-prepared AuNP/GO/PEDOT-PSS/ITO electrode and the electrolyte interface have been characterized through EIS technique, performed within the frequency range, 1 Hz - 1 MHz in PBS electrolyte with a small signal of ac typically 10 mV. Impedance data were fitted with equivalent circuit which consists of one R parallel Constant Phase Element (CPE) in series with another CPE parallel Warburg resistance and series resistance: R_1 represents series resistance, R_{ct} is the charge transfer resistance at the electrode electrolyte interface and W_3 is the Warburg impedance representing diffusion resistance. Q_2 represent the space charge layer contribution at the electrode/electrolyte interface and Q_3 of large magnitude represent the space charge layer between PEDOT rich and PSS rich grains. The measured impedance spectra and fitted impedance spectra of the AuNP/GO/PEDOT-PSS electrodes after various process steps of AF-B_1 sensing like glutaraldehyde treatment, antibody (anti-AF-B_1) immobilization and antibody-analyte interaction for AuNP/GO/PEDOT-PSS/ITO composite electrode, which can be found in Figure 4.7.

The fitted equivalent circuit parameters for the corresponding impedance plots are shown in Table 4.3.

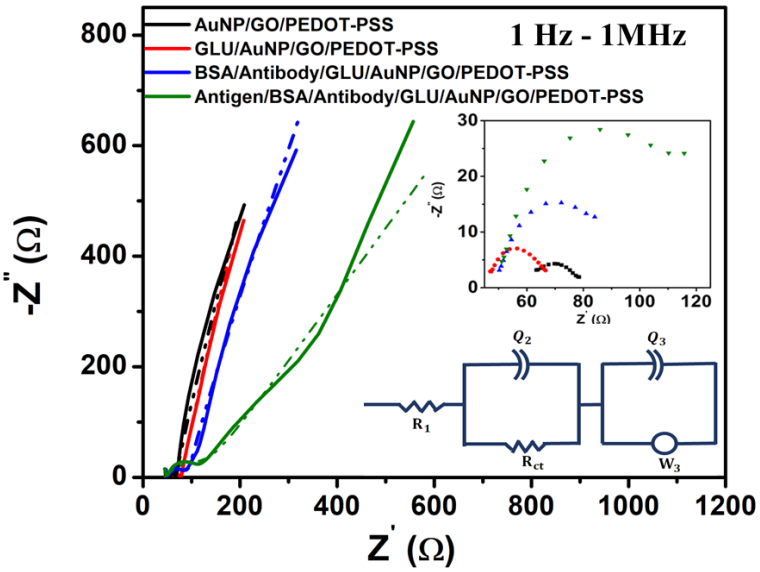

Figure 4.7: Impedance plot of AuNP/GO/PEDOT-PSS films on ITO electrode after each process step and with antigen concentration as a final step in PBS electrolyte. The inset shows the equivalent circuit and high frequency impedance enlarged.

Table 4.3: Fitted parameters of impedance spectra for AuNP/GO/PEDOT-PSS/ITO electrode after every process step and after addition of AF-B_1.

Serial Number	Electrode	R_1 (Ω)	R_{ct} (Ω)	Q_2 ($S.s^n$) (x 10^{-6})	Q_3 ($S.s^n$) (x 10^{-6})	W_3 ($S.s^{1/2}$) (x 10^{-6})
1	AuNP/GO/PEDOT-PSS	63	15	9.560 n=0.419 Q_2^n= 2.575	31.22 n=0.758 Q_3^n= 13.57	95.32
2	GLU/AuNP/GO/ PEDOT-PSS	46.95	20.25	17.22 n= 0.529 Q_2^n= 4.506	2790 n=0.869 Q_3^n= 986.8	289
3	BSA/Antibody / GLU/AuNP/GO/ PEDOT-PSS	45.23	45.38	30 n=0.790 Q_2^n= 14.68	1780 n=0.845 Q_3^n=557.96	340.9
4	Antigen/BSA/Anti-body/GLU/AuNP/ GO/PEDOT-PSS	43.28	85.85	198.2 n=0.524 Q_2^n= 15.98	1614 n=0.563 Q_3^n= 63.98	738.1

The fit parameters revealed that Q_3 increases significantly after glutaraldehyde treatment but reduces after antibody immobilization and followed by antibody-antigen interactions. This would suggest space charge layer modifications between PEDOT and PSS with antibody (anti-AF-B_1) immobilization and antigen (AF-B_1) interaction. After glutaraldehyde treatment the R_{ct} value increases to 20.25 Ω from 15 Ω which may be due to adsorption of the cross linker over the surface of the AuNPs embedded electrode. The charge transfer resistance again increases to 45.38 Ω after immobilization of antibody over the surface of GLU/AuNP/GO/PEDOT-PSS/ITO electrode. As antibody blocks the active sites of the electrode surface and hinders the charge transfer from the electrode surface forming some dielectric layer, enhancement in the R_{ct} value is observed. Further increase in charge transfer resistance value is observed after addition of analyte which confirms the formation of antibody- antigen complexes. Warburg impedance increases after each process steps resulting enhancement in the diffusion impedance. Again, slight increase in

the Q_2 value is observed after antibody-analyte interaction which leads to confirmational changes in the antibody-antigen protein complex structure.

4.6. Capacitive immunosensing of AF-B_1

The impedance response of a particular kinetic phenomenon depends on its characteristic time constants related to frequency of the ac signal. Therefore, multi frequency impedance study was carried out on the sensor which showed wide variations in impedance at frequencies below 10 kHz. Interfacial electrochemical reactions and space charge layer thickness variations/double layer charging effects are strongly dependent on frequency of the ac signal which falls in the frequency range of 50–10 kHz. To study the performance of the immunosensor towards detection of AF-B_1 transient capacitance measurement was carried out both at medium and low frequency such as 77 Hz and 1 kHz. For a label free immunosensor, the maximum capacitive change at the interface during binding of analyte with antibody is monitored directly in transient capacitance plot [43,44]. Transient capacitance measurement has been performed at DC bias voltage 0.8 V, for both 77 Hz and 1 kHz [45]. The transient capacitance was recorded for AuNP/GO/PEDOT-PSS/ITO electrode using two different antibodies, mouse IgG and anti-AF-B_1. The transient capacitance plots for mouse IgG/GLU/ AuNP/GO/PEDOT-PSS/ITO electrode at 77 Hz and 1 kHz is shown in Figure 4.8 (a) and (b) respectively.

After obtaining a stable baseline different concentrations of antigenic solution were added. The baseline shows systematic decrease in capacitance at each subsequent addition of analyte. For selectivity test, the sensor was treated with a non-specific protein molecule named as BSA (40 μg mL^{-1}), as shown in Figure 4.8 (a,b). At 77 Hz, the sensor did not exhibit any observable changes while BSA was added. While at 1 kHz, upon addition of BSA, the baseline increases but suddenly decreases to retain its earlier trend, resulting in high selectivity of the proposed immunosensor.

To obtain a sensor response vs. antigen concentration plot, the transient capacitance change (ΔC_p) for the mouse IgG/GLU/AuNP/GO/PEDOT-PSS/ITO electrode with respect to concentration of antigen (ΔConc.) at each subsequent addition for both 77 Hz and 1 kHz respectively are shown in Figure 4.8 (c). Interestingly, at 77 Hz, the sensor depicted a rapid increase from 18.18 to 35 ng mL^{-1} followed by a steady

response from 35 ng mL^{-1} to 300 ng mL^{-1}. The sensor showed two concentration ranges within 18.18-35 ng mL^{-1} and 35-291.42 ng mL^{-1} at 1 kHz.

By employing the equation of adsorption isotherm [45]

$$Y = \frac{A}{1+\frac{B}{x}} \tag{4.3}$$

concentration vs. capacitance variation was fitted. In this equation, x represents change in antigen concentration, and Y represents the change in capacitive response. Both A and B are constants, A being the response of the saturated capacitance while B represents inverse of the adsorption coefficient.

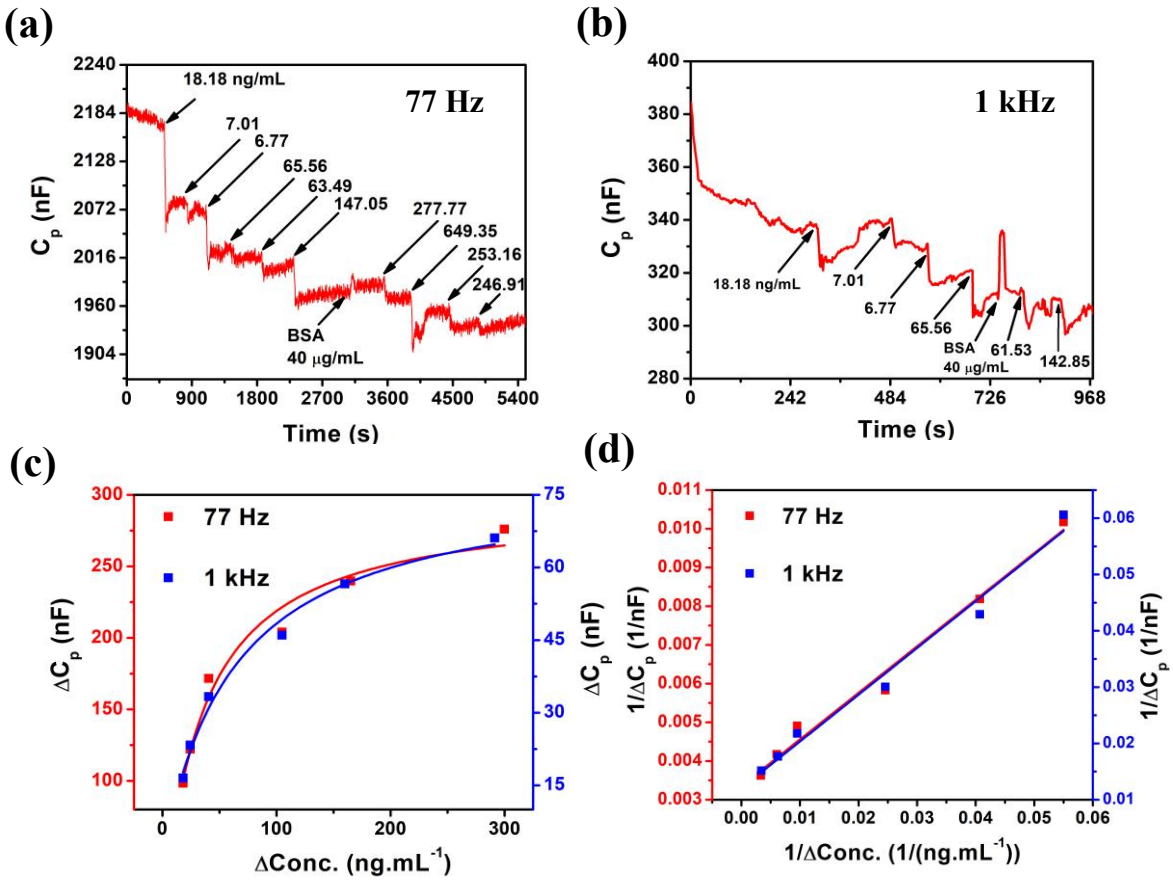

Figure 4.8: Transient capacitance plot of mouse IgG/GLU/AuNP/GO/PEDOT-PSS based immunosensor at (a) 77 Hz, (b) 1 kHz towards detection of anti-AF-B_1 raised in mouse. (c) Langmuir plot of mouse IgG/GLU/AuNP/GO/PEDOT-PSS sensors at 77 Hz and 1 kHz. (d) Linear regression plot of mouse IgG/GLU/AuNP/GO/PEDOT-PSS capacitive sensor at 77 Hz and 1 kHz.

By fitting the sensors response curve with the adsorption isotherm, and plotting $1/\Delta C_p$ vs. $1/\Delta$Conc., a linear calibration plot for a wider sensing range for AF-B_1 sensor can be obtained (Figure 4.8 (d)). The respective LODs were calculated and found to be 67.75 ng mL^{-1} at 77 Hz and 62.5 ng mL^{-1} at 1 kHz. The immunosensor showed a sensitivity of 8.31 $nFng^{-1}mL$ at 77 Hz and 1.20 $nFng^{-1}mL$ at 1 kHz. The repeatability of the mouse IgG/AuNP/GO/PEDOT-PSS sensor was assessed by following same process steps, and the findings are presented in Table 4.4. These results, obtained through transient capacitance measurements, indicate a high degree of repeatability, demonstrating the reliability of the sensor. Specifically, the sensor exhibited a LOD of approximately 60.0 ng mL^{-1} at a frequency of 77 Hz and around 69.0 ng mL^{-1} at 1 kHz, emphasizing its sensitivity in detecting low analyte concentrations. Additionally, the linear regression plots for this sensor, with corresponding error bars, at the two frequencies of 77 Hz and 1 kHz is illustrated in Figure 4.9. This results further confirms that the sensor performs consistently at both frequencies, demonstrating its strong and reliable detection abilities.

Table 4.4: Results from repeated experiments for mouse IgG/GLU/AuNP/GO/PEDOT-PSS capacitive mouse derived anti-AF-B_1 sensor (both at 77 Hz and 1 kHz).

Serial number	Electrode	Frequency, Hz	LOD, (ng mL^{-1})	Sensitivity, ($nFng^{-1}mL$)	Linear range, (ng mL^{-1})
1	AuNP/GO/PEDOT -PSS, sensor 1	77	67.75	1/0.12032 = 8.311	18.18-300
2	AuNP/GO/PEDOT -PSS, sensor 2	77	58.82	1/0.19028 =5.2631	18.18-300
3	AuNP/GO/PEDOT -PSS, sensor 3	77	52.63	1/0.13109 =7.6923	18.18-300
4	AuNP/GO/PEDOT -PSS, sensor 1	1000	62.5	1/0.83069 =1.2038	18.18-291.42
5	AuNP/GO/PEDOT -PSS, sensor 2	1000	68.49	1/0.795 =1.2578	18.18-291.42
6	AuNP/GO/PEDOT -PSS, sensor 3	1000	76.46	1/0.8906 =1.1228	18.18-291.42

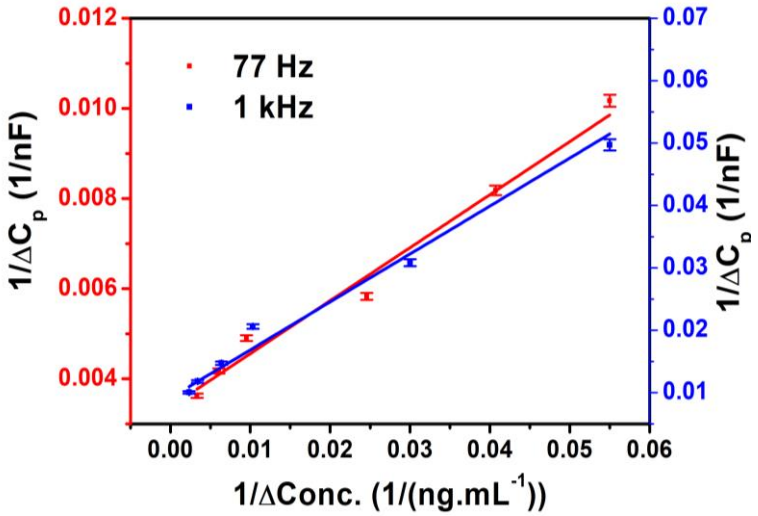

Figure 4.9: Linear regression plot of mouse IgG/GLU/AuNP/GO/PEDOT-PSS capacitive sensors at 77 Hz and 1 kHz with error bar towards detection of mouse derived anti-AF-B_1.

The inclusion of the mouse IgG antibody-based sensor in this section served as an essential preliminary step to evaluate the immunosensing performance of Au/GO/PEDOT-PSS platform. In the initial phase, mouse IgG was immobilized onto the sensor surface to detect its specific target, anti-AF-B_1 antibody which is raised in mouse, as a model antigen–antibody pair. This was done to validate the immobilization strategy, probe–target interaction, and capacitive signal response of the developed sensing interface. Following the effective demonstration of sensitive and specific detection using this model immunosystem, we proceeded to functionalize the same Au/GO/PEDOT-PSS platform with anti-AF-B_1 antibodies for the selective capacitive detection of AF-B_1. This progression ensured the reliability and reproducibility of the sensor system before deploying it for real-target (AF-B_1) detection. Thus, the mouse IgG-based sensor served as a model validation step, confirming the platform's suitability for label-free capacitive immunosensing, and justifying its subsequent application for AF-B_1 detection using anti-AF-B_1 antibodies.

The transient capacitance plot for the anti-AF-B_1/GLU/AuNP/GO/PEDOT-PSS/ITO electrode at 77 Hz is shown in Figure 4.10 (a) and the plot at 1 kHz can be found in Figure 4.11 respectively, which suggested the optimum frequency for monitoring antigen antibody interactions of a capacitive immunosensor based on the PEDOT-PSS composite electrode. As the interface between the electrode and electrolyte in the

electrochemical cell functions as an electrolytic capacitor, each subsequent addition of AF-B_1 causes specific binding with immobilized antibody resulting in the capacitive response due to changes in the dielectric layer thickness. After obtaining a stable baseline, a systematic decrease in the capacitance was observed after each addition of the analyte (Figure 4.10 (a)).

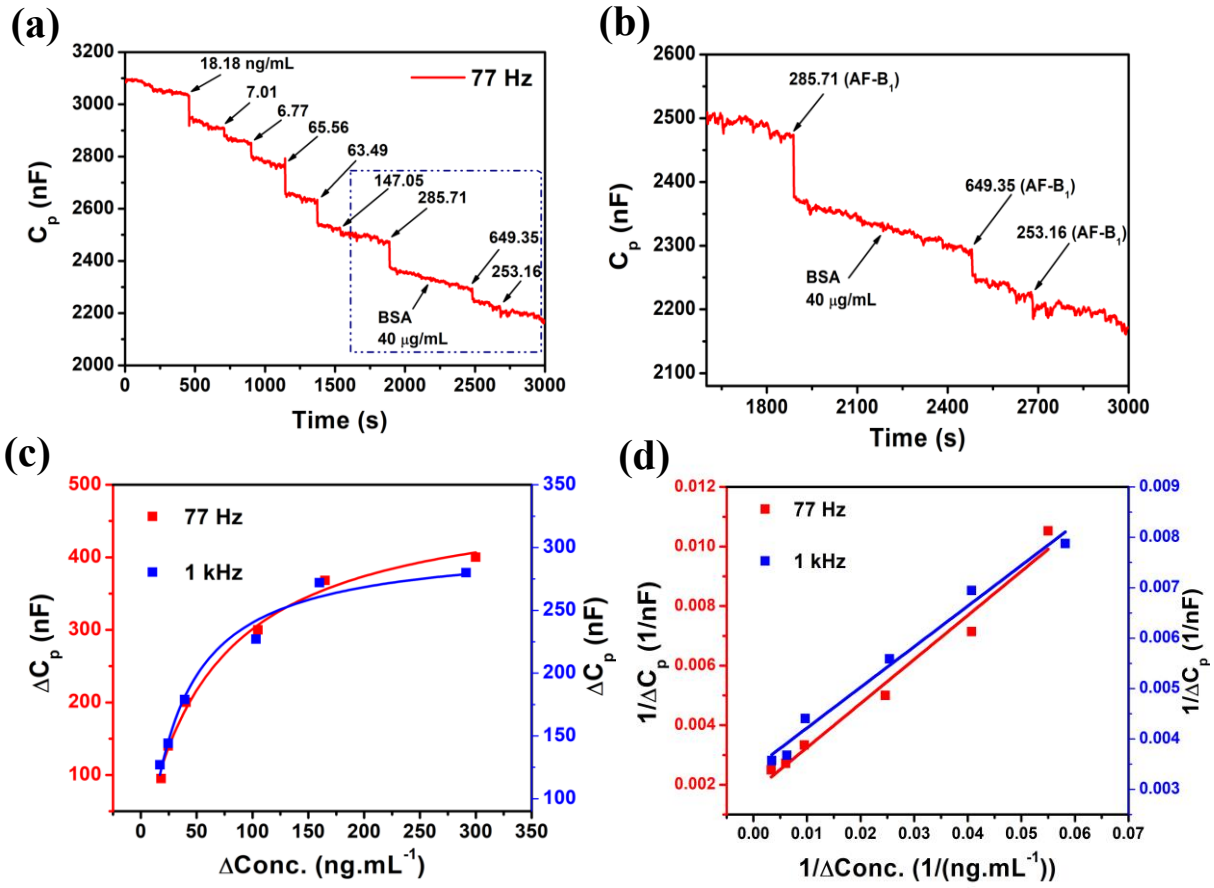

Figure 4.10: Transient capacitance plot of anti-AF-B_1/GLU/AuNP/GO/PEDOT-PSS based AF-B_1 sensors at (a) 77 Hz at a DC bias voltage of 0.8 V (b) Selectivity test. (c) Adsorption plot and (d) Linear regression plot of anti-AF-B_1/GLU /AuNP/GO/PEDOT-PSS capacitive sensor at 77 Hz and 1 kHz.

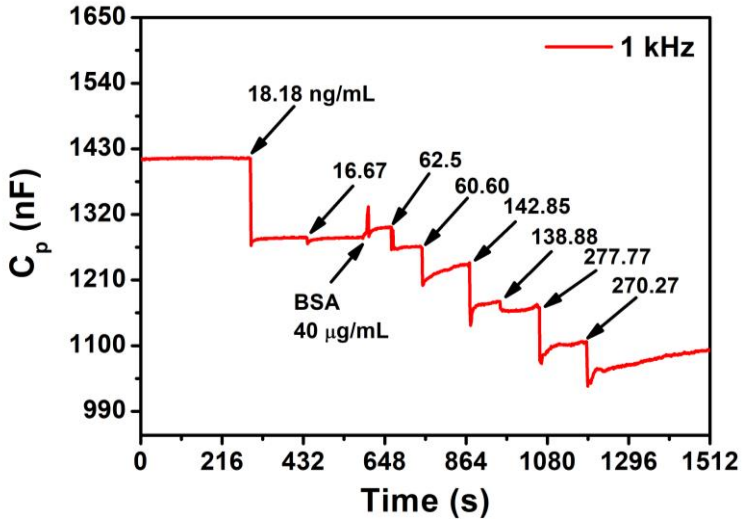

Figure 4.11: Transient capacitance plot of anti-AF-B_1/GLU/AuNP/GO/PEDOT-PSS based AF-B_1 sensors at 1 kHz.

To evaluate the selectivity of the proposed immunosensor non-specific protein molecule namely, (40 µg mL^{-1}) BSA (~68 KDa) was injected while the immunosensor exhibited no appreciable change in capacitance indicating the proposed capacitive biosensor is highly selective to the specific analyte (Figure 4.10 (b)). The change in transient capacitance (ΔC_p) for the anti-AF-B_1/GLU/AuNP/GO/PEDOT-PSS/ITO electrode with respect to concentration of antigen (ΔConc.) at each subsequent addition for both the frequency is shown in Figure 4.10 (c). We observed that in the concentration range, 18.18-88.0 ng mL^{-1} the capacitance response increases rapidly till saturation in the range of 88.0-300.0 ng mL^{-1} at a frequency of 77 Hz (Figure 4.10 (c)). Further the capacitive change with respect to antigenic concentration for both the frequency, 77 Hz and 1 kHz is plotted and fitted using adsorption isotherm, equation 4.3, shown in Figure 4.10 (c). Linear regression was plotted for inverse of capacitance change with respect to inverse of concentration change for both the frequency and shown in Figure 4.10 (d). The respective LODs [36] are estimated to be, 55.41 ng mL^{-1} (77 Hz), and 62.45 ng mL^{-1} (1 kHz). The sensitivity of the immunosensor was calculated to be 6.76 $nFng^{-1}mL$ and 12.40 $nFng^{-1}mL$ both at 77 Hz and 1 kHz; respectively. Hence transient capacitance studies at both frequencies are suitable 77 Hz is more preferred with a lower LOD. We have thus achieved a wider concentration range for detection of AF-B_1 in comparison to other reported works [46-49].

Table 4.5: Results from repeated experiments for AF-B_1 capacitive sensor (both at 77 Hz and 1 kHz).

Serial number	Electrode	Frequency, Hz	LOD, (ng mL^{-1})	Sensitivity, ($nFng^{-1}mL$)	Linear range, (ng mL^{-1})
1	AuNP/GO/PEDOT -PSS, sensor 1	77	55.41	1/0.1479 = 6.76	18.18-300.0
2	AuNP/GO/PEDOT -PSS, sensor 2	77	55.86	1/0.0857 =11.66	18.18-300.0
3	AuNP/GO/PEDOT -PSS, sensor 3	77	57.50	1/0.1902 =5.25	18.18-300.0
4	AuNP/GO/PEDOT -PSS, sensor 1	1000	62.45	1/0.0806 =12.40	18.18-291.42
5	AuNP/GO/PEDOT -PSS, sensor 2	1000	62.97	1/0.2995 =3.33	18.18-291.42
6	AuNP/GO/PEDOT -PSS, sensor 3	1000	61.61	1/1.7871 =0.56	18.18-291.42

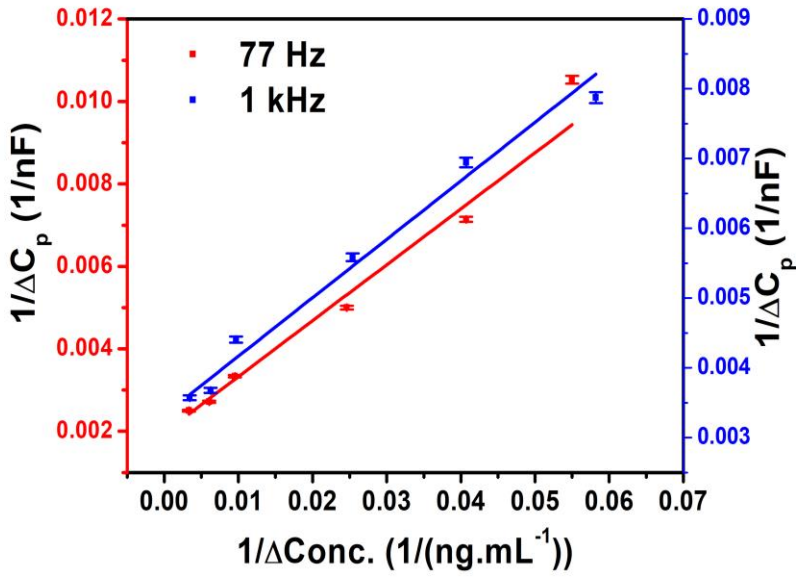

Figure 4.12: Linear regression plot of anti-AF-B_1/GLU/AuNP/GO/PEDOT-PSS capacitive sensors at 77 Hz and 1 kHz with error bar.

Furthermore, repeatability has been checked for the anti-AF-B_1/AuNP/GO/PEDOT-PSS sensor by employing similar process steps and the obtained results from transient capacitance measurements are presented in Table 4.5. It shows very good repeatability with LOD value, ~50.0 ng mL^{-1} at 77 Hz and ~65.0 ng mL^{-1} at 1 kHz. The linear regression plots of the same sensor with error bars at 77 Hz and 1 kHz are shown in Figure 4.12; respectively.

4.7. AF-B_1 sensor response using Differential Pulse Voltammetry

Another investigation of the electrochemical response of the immunosensor was carried out using the DPV method, a sophisticated electrochemical technique that can be utilized to study the electrochemical amperometric responses. As part of a DPV, a series of voltage pulses are superimposed on stair-step patterns to polarize the working electrode. The current is monitored before and after each potential step, and the changes in the currents of the pulse obtained after and before are utilized as the signal. Using such a procedure minimizes the capacitive current contribution owing to the injection/extraction of holes and the exchange of ions with solutions during the charging of PEDOT – PSS [50]. As a result, it provides the opportunity to measure the faradic current associated with the reaction between the antibody and the target analyte. DPV was performed for BSA/anti-AF-B_1/GLU/AuNP/GO/PEDOT- PSS/ITO electrode within the potential window -0.2 V to 0.8 V in 100 mM phosphate buffer and 5 mM $[Fe(CN)_6]^{3-/4-}$ (Figure 4.13 (a)). As the concentration of AF-B_1 increases, the peak current decreases proportionally, suggesting that AF-B_1 interacts specifically with the anti-AF-B_1. Apparently, upon formation of antigen and antibody complex on the electrode, it could efficiently prevent the transfer of electrons from the redox probe $[Fe(CN)_6]^{3-/4-}$ to the electrode. The selectivity of the immunosensor was studied by injecting (40 μg mL^{-1}) BSA (non-specific) and is shown in Figure 4.13 (b). The sensor exhibited no shift or change in peak current after addition of BSA resulting in excellent selectivity of the proposed immunosensor.

Change in peak current for the BSA/anti-AF-B_1/GLU/AuNP/GO/PEDOT-PSS/ITO electrode with respect to concentration of antigen can be found in Figure 4.13 (c). In the concentration range, 18.18 - 87.55 ng mL^{-1} the current response increases rapidly till slow saturation in the range of 87.55-342.85 ng mL^{-1}.

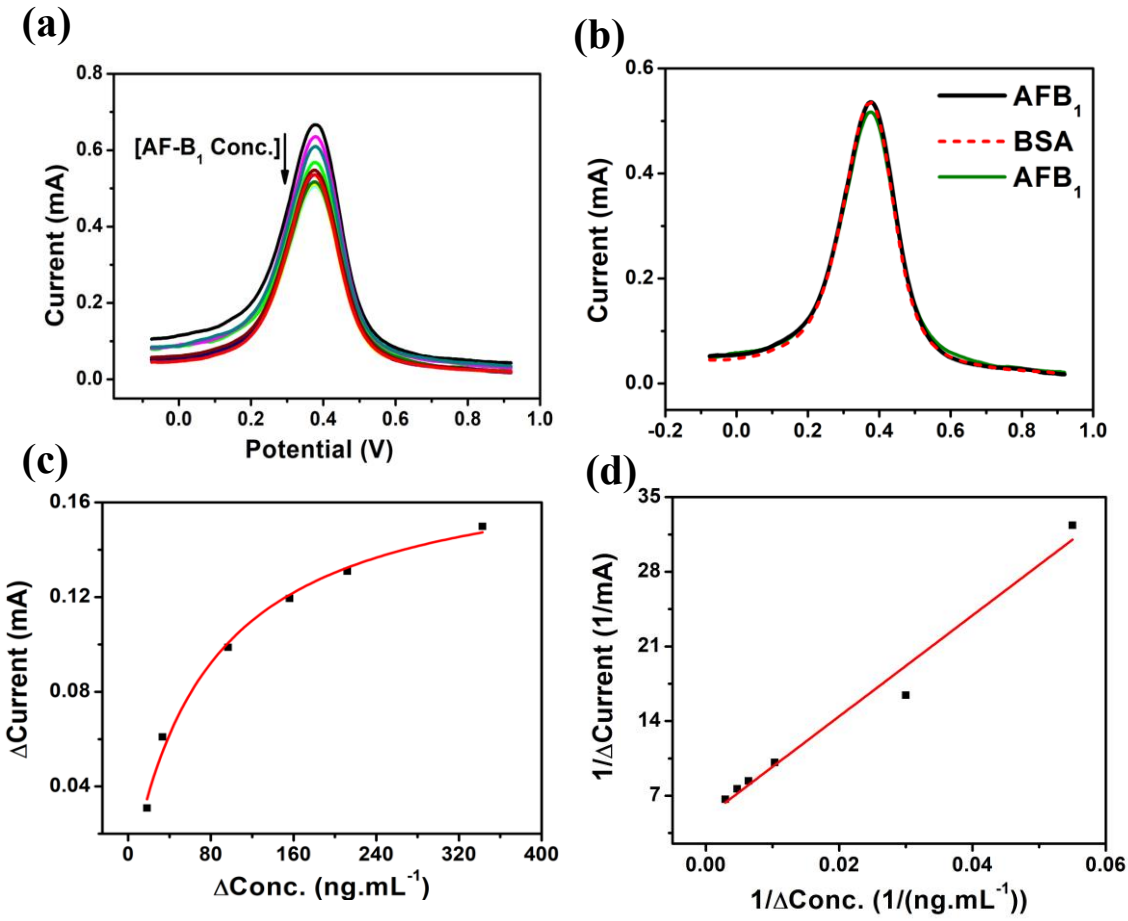

Figure 4.13: DPV plot of BSA/anti-AF-B_1/GLU/AuNPs/GO/PEDOT-PSS/ITO with concentration of AF-B_1 (18.18 ng mL^{-1}-594.59 ng mL^{-1}) within potential window -0.2 V to 0.8 V. (b) Selectivity test. (c) Adsorption isotherm fitted for change in peak current of DPV with change in antigen concentration. (d) Linear regression fitting for 1/ΔConc. vs. 1/ΔCurrent from DPV response.

By employing the equation of adsorption isotherm (equation 4.3) concentration vs. current variation was fitted. Here, *x* is change in antigen concentration and *Y* represents the change in current response. Both *A* and *B* are constants, *A* being the response of the saturated current while *B* represents inverse of the adsorption coefficient. By fitting Figure 4.13 (c) with the adsorption isotherm, and plotting 1/ΔCurrent vs. 1/ΔConc., a linear calibration plot for a wider sensing range for AF-B_1 sensor was obtained (Figure 4.13 (d)). The LOD [36] was estimated as 65.29 ng mL^{-1} (435 pM) with a response of 1/473.41=2.112 μAng^{-1}mL. Furthermore, repeatability has been checked for other AuNP/GO/PEDOT-PSS

sensors and the obtained results are presented in Table 4.6 and the linear regression plot of the same sensor with error bars can be found in Figure 4.14. Data shows very good repeatability with LOD value, 60-120 ng mL^{-1} (400-800 pM). Both capacitive and differential pulse voltammetry methods showed comparable results.

Table 4.6: Results from repeated experiments for anti-AF-B_1/GLU/AuNP/GO/PEDOT-PSS based AF-B_1 sensor using DPV.

Serial number	Electrode	LOD, (ng mL^{-1})	Sensitivity, ($\mu Ang^{-1}mL$)	Linear range, (ng mL^{-1})
1	AuNP/GO/PEDOT-PSS, sensor 1	65.29	1/473.41 =2.112	18.18-342.85
2	AuNP/GO/PEDOT-PSS, sensor 2	60.33	1/477.98 =2.092	18.18-342.85
3	AuNP/GO/PEDOT-PSS, sensor 3	119.51	1/533.56 =1.874	18.18-342.85

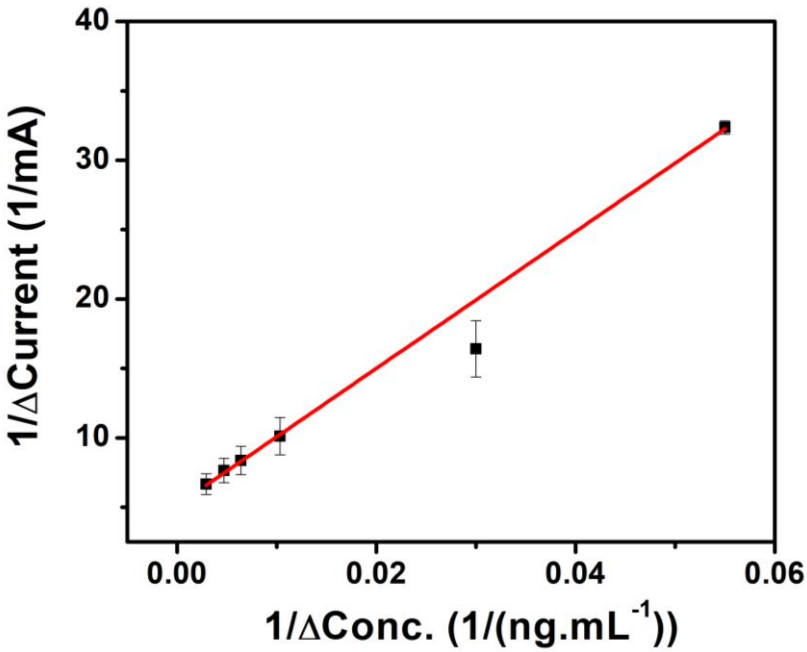

Figure 4.14: 1/ΔI vs. 1/ΔConc for the BSA/anit-AF-B_1/GLU/AuNP/GO/PEDOT-PSS sensor along with linear regression plot with error bar w.r.to standard deviation.

4.8. Performance of the Aflatoxin sensor towards real sample

In order to implement the proof of concept for real samples, DPV was carried out on BSA/anti-AF-B_1/GLU/AuNP/GO/PEDOT-PSS/ITO immunosensor with real samples (white button Mushroom, scientific name: *Agaricus bisporus*, purchased from local market, Geographic location: Delhi and Okra, scientific name: *Abelmoschus esculentus*, purchased from Local market).

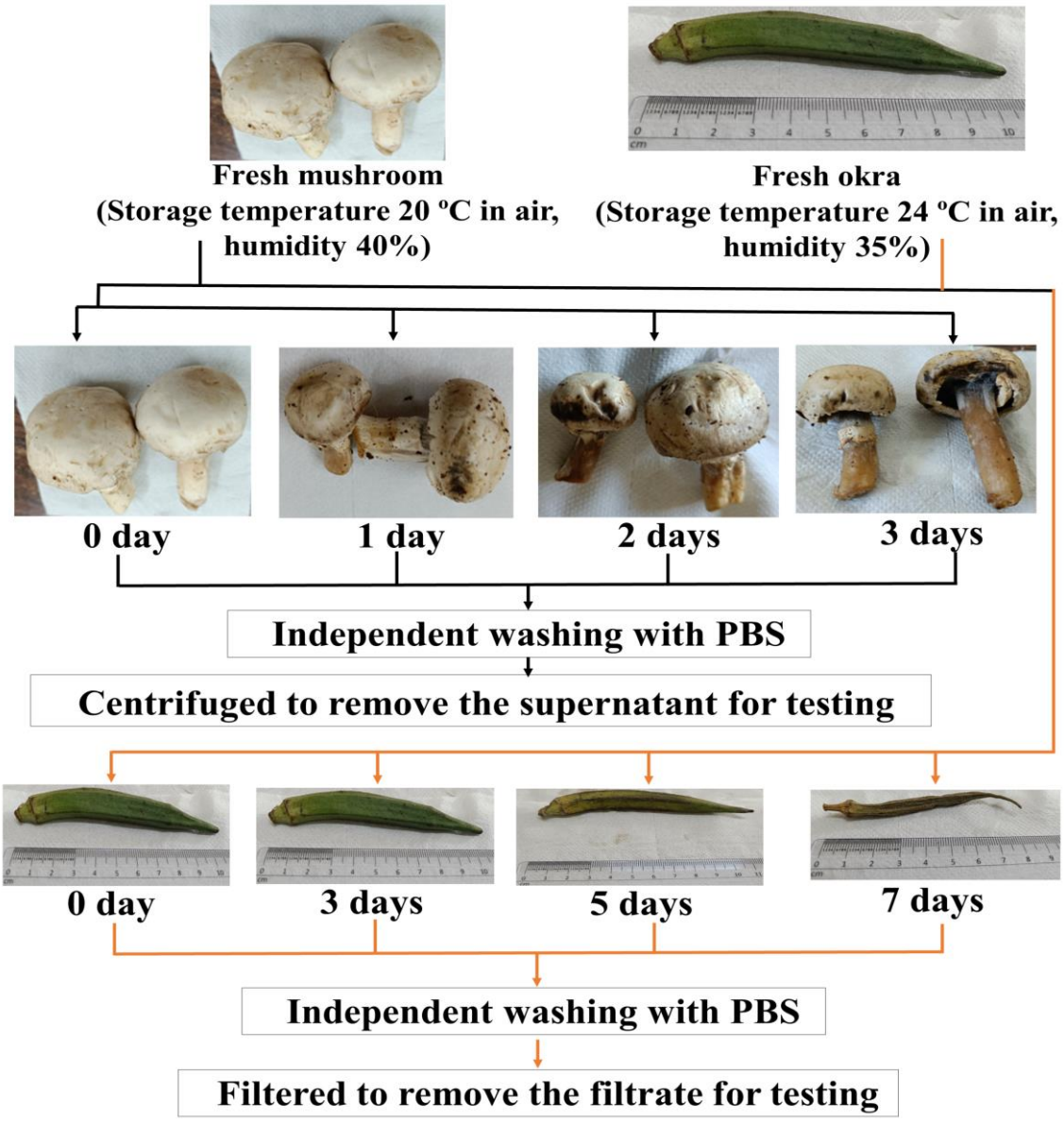

Figure 4.15: Scheme for testing white button Mushroom, Okra of different days of air exposure at 20-24 ºC after purchase.

Freshly harvested mushroom is highly perishable as it is susceptible to deterioration by the microorganisms and enzyme as they become susceptible to mold, bacteria, and loss of the active ingredients. The shelf life may be extended by refrigeration at 1-4 °C. Schematic representing preparation of real samples (mushrooms and okra) for testing, is shown in Figure 4.15. Here for our study, mushrooms were kept at a temperature of 20 ºC in air (humidity 40%) for one, two and three days. The DPV was recorded with PBS used for washing fresh mushroom as well as one, two and three days older mushrooms with repeated spiking (50-300 µL). SEM micrograph of as purchased and mushroom stored for 3 days at ambient conditions are shown in Figure 4.16 (a) and (b); respectively. Three days older mushroom shows *conidiophore* and *mycelial* morphology of *Aspergillus flavus* confirming contamination of AF-B_1 [51]. On the other hand, okra was kept at 24 ºC in air (humidity 35%) for three, five and seven days. The DPV was recorded with PBS used for washing fresh okra as well as three, five and seven days older okra with different spiking (50-300 µL).

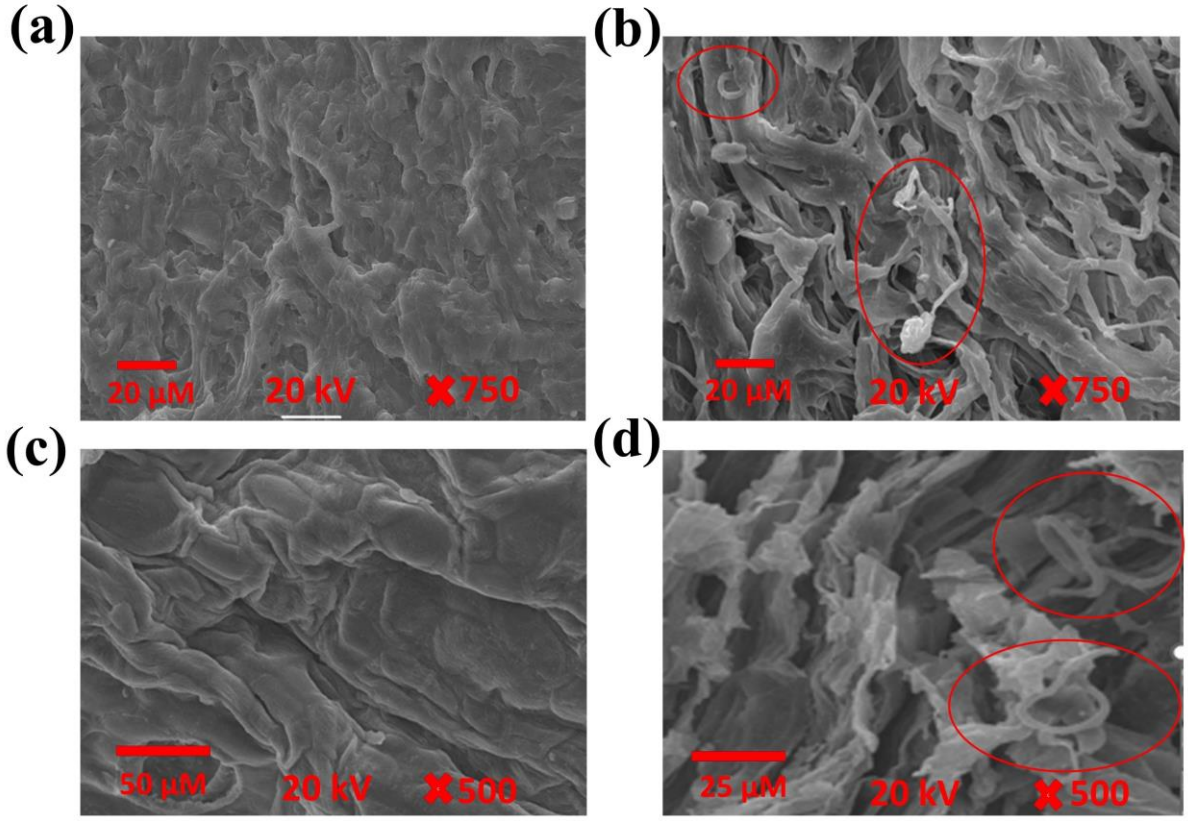

Figure 4.16: SEM images of (a) as purchased mushroom, (b) 3 days stored mushroom, (c) as purchased okra (d) 7 days stored okra.

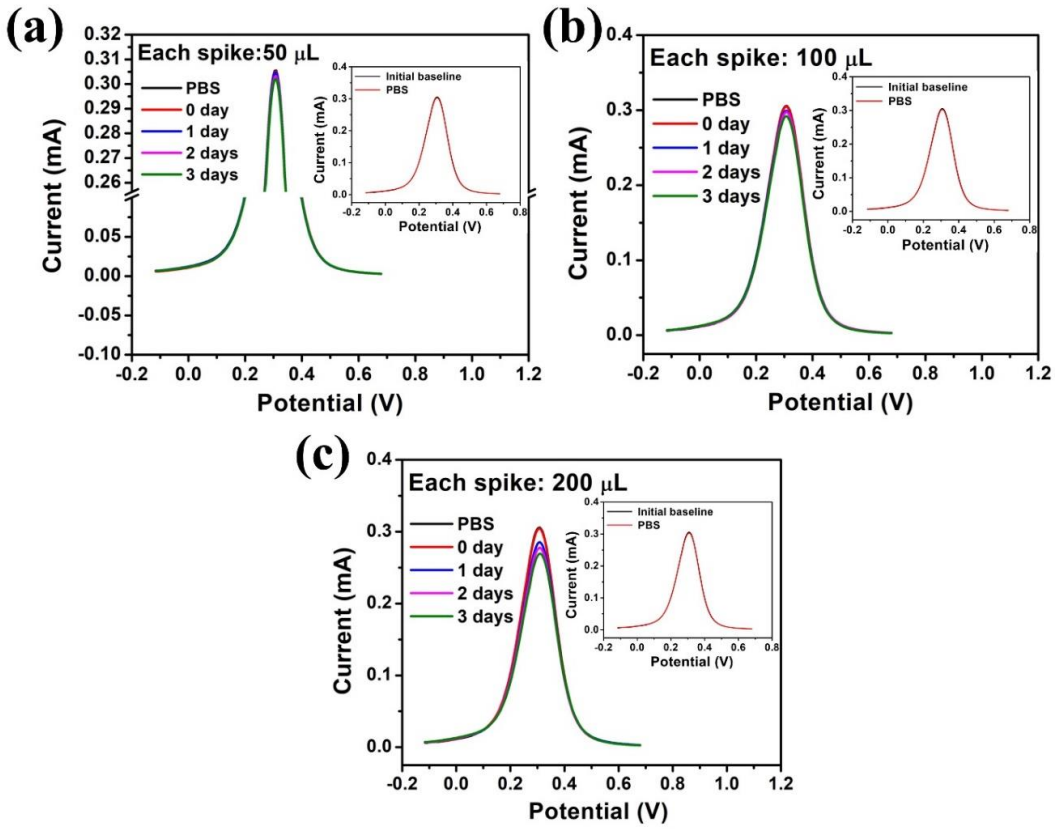

Figure 4.17: DPV pattern of AuNP/GO/PEDOT-PSS/ITO composite electrode towards mushrooms (kept exposed to air 20 ºC for 0-3 days and washed with PBS) with different spiking volumes (50-200) µL, (a) 50 µL (b) 100 µL, (c) 200 µL. Inset shows the voltammogram after addition of 200 µL PBS.

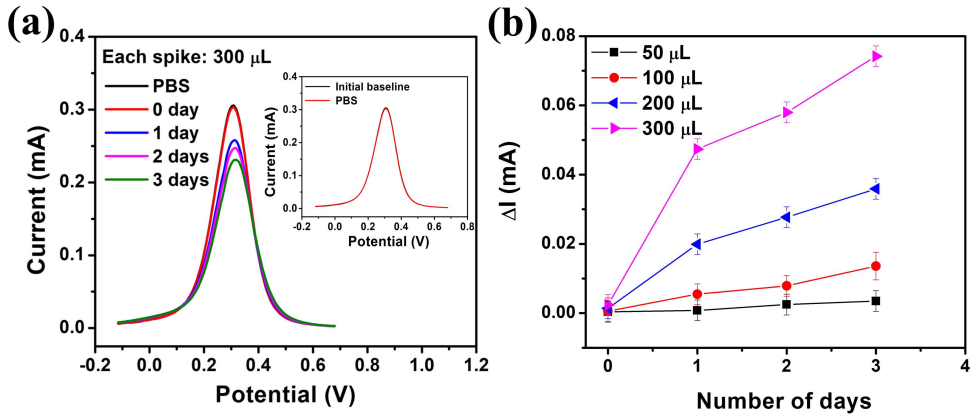

Figure 4.18: (a) DPV pattern of AuNP/GO/PEDOT-PSS/ITO composite electrode towards mushrooms (kept exposed to air 20 ºC for 0-3 days and washed with PBS) with spiking volumes 300 µL. Inset shows the voltammogram after addition of 200 µL PBS. (b) Change in peak current vs number of days of air exposure for mushrooms.

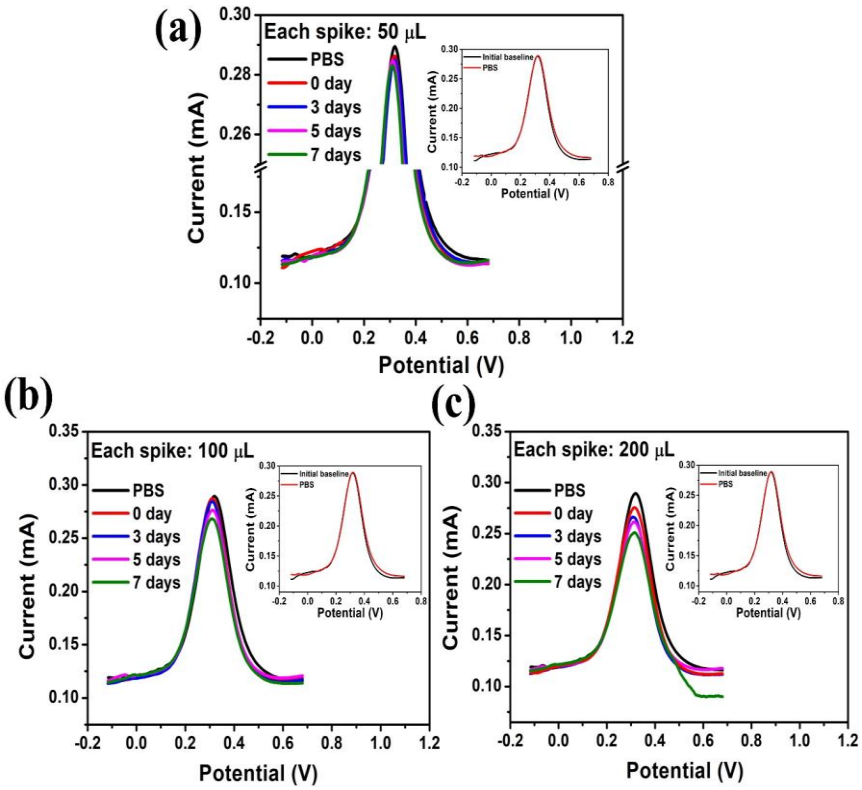

Figure 4.19: DPV pattern of AuNP/GO/PEDOT-PSS/ITO composite electrode towards okra (kept exposed to air 24 ºC for 0-7 days and washed with PBS) with different spiking volumes (50-200) µL, (a) 50 µL (b) 100 µL, (c) 200 µL. Inset of each figure shows the voltammogram after addition of 200 µL PBS.

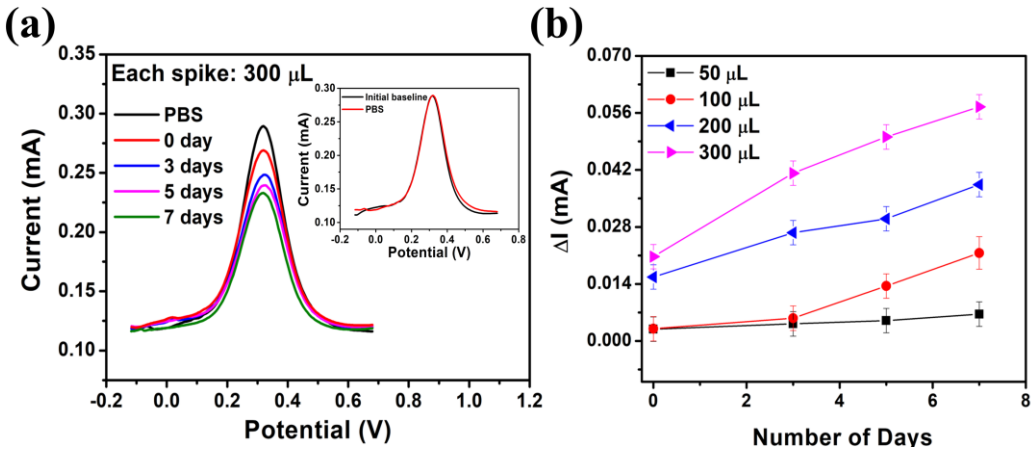

Figure 4.20: (a) DPV pattern of AuNP/GO/PEDOT-PSS/ITO composite electrode towards okra (kept exposed to air 24 ºC for 0-7 days after purchase and washed with PBS) with spiking volumes 300 µL. Inset shows the voltammogram after addition of 200 µL PBS. (b) Change in peak current vs number of days of air exposure for okra.

The DPV current response for mushrooms of different days of air exposure with repeated spiking of (50-200 µL) is shown in Figure 4.17 (a-c) respectively and DPV current response with spiking 300 µL can be found in Figure 4.18 (a). Further, change in the DPV peak current for each spike as a function of number of days is shown in Figure 4.18 (b), which suggested presence of 52.30 ng mL^{-1} AF-B_1 in mushroom after 3 days of exposure at room temperature.

DPV current response for different days of air exposed okra with different spiking like 50, 100, 200 µL is shown in Figure 4.19 (a-c) respectively and corresponding current response with repeated spiking like 300 µL can be found in Figure 4.20 (a). Further, change in the DPV peak current for each spike as a function of number of days is shown in Figure 4.20 (b) which showed presence of 40.28 ng mL^{-1} AF-B_1 in okra after 7 days of exposure at room temperature. It may be concluded that the immunosensor is suitable for detecting AF-B_1 in real samples without any obstruction or interference.

To be mentioned, Kamal et al. detected AF-B_1 in Fresh as well as different processed mushrooms using chromatography technique [52]. In the sample preparation technique, first they have blended the mushrooms followed by addition of distilled water and acetone in order to make it soluble. Then the solution was shacked for about 30 minutes followed by filtration and then concentrated under nitrogen gas. Afterwards, a vacuum manifold was used to extract the solid phase from the solution. The extract was diluted with methanol, acetonitrile and deionized water as a final step and injected into HPLC. The group has found 5.53282 µg.kg^{-1} of aflatoxin B_1 presence in canned Button mushrooms [52]. Comparatively our sample preparation approach is easy and simple requiring only washing and filtering/centrifuging.

4.9. Conclusions

PEDOT-PSS, GO/PEDOT-PSS and AuNP/GO/PEDOT-PSS were studied for highly sensitive, selective and user friendly glucose sensing and AF-B_1 sensing using *GlOx*/GLU/AuNP/GO/PEDOT-PSS/ITO and anti-AF-B_1/GLU/AuNP/GO/PEDOT-PSS/ITO electrodes respectively. Electrochemical techniques such as, CV, amperometry, DPV and EIS were employed for sensor characterization and data analyses. Immobilization of glucose oxidase enzyme over the electrode in presence of

glutaraldehyde was confirmed by corresponding change in the impedance and CV plots. Multifrequency impedance spectra measurements of the respective electrodes and their fitted equivalent circuit parameters helped to understand the various interfacial charge transfer mechanisms. The entrapped *GlOx* enzyme exhibited good linearity towards oxidation of glucose on Au/GO/PEDOT-PSS sensor. Repeatability of the sensor electrodes were tested using few glucose sensors. The direct, glucose sensor based on Au/GO/PEDOT-PSS offered a wider linearity in the range 3.84-373.33 μA μM^{-1} with a LOD value of 2.33 μM. The developed glucose sensors were finally tested in human saliva samples yielding reliable performance with excellent repeatability. Importantly, the use of AuNP/GO/PEDOT-PSS/ITO provided distinct advantages over conventional carbon-based electrodes (e.g., glassy carbon or carbon paste electrodes). While conventional electrodes often suffer from limited sensitivity, poor enzyme immobilization efficiency, and inefficient electron transfer, the engineered nanocomposite system in this study integrated the catalytic properties of gold nanoparticles, the high surface area and functional groups of graphene oxide, and the excellent conductivity and film-forming ability of PEDOT-PSS. This effective combination led to enhanced electrochemical performance, improved sensor stability, and a lower detection limit. Although the working potential is relatively high, the composite architecture leads to a synergistic enhancement in performance, especially in terms of sensor stability, reproducibility, and signal amplification. Moreover, the modified electrode shows a low limit of detection, wide linear range, and good selectivity toward glucose from saliva, even in the presence of common interfering substances, which is often challenging for bare carbon electrodes. As for AF-B_1 detection, the immunosensor mouse IgG/GLU/AuNP/GO/PEDOT-PSS showed LOD's 67.75 ng mL^{-1} at 77 Hz and 62.5 ng mL^{-1} at 1 kHz. The sensitivity was found to be of 8.31 $nFng^{-1}mL$ and 1.20 $nFng^{-1}mL$ both at 77 Hz and at 1 kHz with a concentration range within 18.18-300.0 ng mL^{-1}. The anti-AF-B_1/GLU/AuNP/GO/PEDOT-PSS immunosensor, displayed linearity for 18.18-342.85 ng mL^{-1} with response of 2.112 $\mu Ang^{-1}mL$ and LOD 65.29 ng mL^{-1} (435 pM). From capacitive response, the sensor displayed a LOD of 55.41 ng mL^{-1} (369 pM) at 77 Hz with linearity within 18.18-300.0 ng mL^{-1} and 62.45 ng mL^{-1} (416 pM) at 1 kHz within the range of 18.18-291.42 ng mL^{-1}. Repeatability of the sensor electrodes were tested using few AF-B_1 sensors for both methods. AF-B_1 sensor has been tested with fresh and few days air exposed white button mushrooms and okra (washed with

PBS) which showed linear variations of DPV signal suggesting direct application. In this study, we have compared the use of AuNP/GO/PEDOT-PSS electrodes for label free sensing of AF-B_1 by both capacitive and DPV methods which displayed similar results. The versatility of the AuNP/GO/PEDOT-PSS electrodes have been demonstrated for direct on-site measurements of AF-B_1 and glucose by both transient capacitance and amperometry. Still there is high scope for the improvement of the sensing parameters of the developed biosensors. Next chapter will describe the use of another 2D TMSCs material especially WS_2 in place of GO to further enhance the sensitivity, linearity and LOD of the glucose sensor and AF-B_1 sensor.

4.10. References

[1] Balakumar, P., Maung-U, K., and Jagadeesh, G. Prevalence and prevention of cardiovascular disease and diabetes mellitus. *Pharmacological research*, 113:600-609, 2016.

[2] Hossain, M. J., Al-Mamun, M., and Islam, M. R. Diabetes mellitus, the fastest growing global public health concern: Early detection should be focused. *Health Science Reports*, 7(3):e2004, 2024.

[3] Chou, C. Y., Hsu, D. Y., and Chou, C. H. Predicting the onset of diabetes with machine learning methods. *Journal of Personalized Medicine*, 13(3):406, 2023.

[4] Scognamiglio, V. Nanotechnology in glucose monitoring: Advances and challenges in the last 10 years. *Biosensors and Bioelectronics*, 47:12-25, 2013.

[5] Azimi, S., Farahani, A., Docoslis, A., and Vahdatifar, S. Developing an integrated microfluidic and miniaturized electrochemical biosensor for point of care determination of glucose in human plasma samples. *Analytical and Bioanalytical Chemistry*, 413:1441-1452, 2021.

[6] Usher-Smith, J. A., Thompson, M. J., Sharp, S. J., and Walter, F. M. Factors associated with the presence of diabetic ketoacidosis at diagnosis of diabetes in children and young adults: a systematic review. *Bmj*, 343:d4092, 2011.

[7] Elsherif, M., Hassan, M. U., Yetisen, A. K., and Butt, H. Wearable contact lens biosensors for continuous glucose monitoring using smartphones. *ACS nano*, 12(6):5452-5462, 2018.

[8] World Health Organization. Global health risks: mortality and burden of disease attributable to selected major risks. *World Health Organization*, 2009.

[9] Baena-Diez, J. M., Penafiel, J., Subirana, I., Ramos, R., Elosua, R., Marin-Ibanez, A., ... and FRESCO Investigators. Risk of cause-specific death in individuals with diabetes: a competing risks analysis. *Diabetes care*, 39(11):1987-1995, 2016.

[10] Chauhan, R., Singh, J., Sachdev, T., Basu, T., and Malhotra, B. D. Recent advances in mycotoxins detection. *Biosensors and Bioelectronics*, 81:532-545, 2016.

[11] Singh, A. K., Sri, S., Garimella, L. B., Dhiman, T. K., Sen, S., and Solanki, P. R. Graphene quantum dot-based optical sensing platform for aflatoxin B_1 detection via the resonance energy transfer phenomenon. *ACS Applied Bio Materials*, 5(3):1179-1186, 2022.

[12] Robbins, C. A., Swenson, L. J., Nealley, M. L., Kelman, B. J., and Gots, R. E. Health effects of mycotoxins in indoor air: a critical review. *Applied occupational and environmental hygiene*, 15(10):773-784, 2000.

[13] Sun, C., Liao, X., Jia, B., Shi, L., Zhang, D., Wang, R., ... and Kong, W. Development of a ZnCdS@ ZnS quantum dots–based label-free electrochemiluminescence immunosensor for sensitive determination of aflatoxin B_1 in lotus seed. *Microchimica Acta*, 187:1-9, 2020.

[14] Khansili, N., and Murali Krishna, P. Sensitive metal oxide-clay nanocomposite colorimetric sensor development for aflatoxin detection in foods: Corn and almond. *ACS omega*, 6(23):14911-14925, 2021.

[15] Zuo, J., Yan, T., Tang, X., Zhang, Q., and Li, P. Dual-modal immunosensor made with the multifunction nanobody for fluorescent/colorimetric sensitive detection of aflatoxin B_1 in maize. *ACS Applied Materials & Interfaces*, 15(2):2771-2780, 2023.

[16] Nazhand, A., Durazzo, A., Lucarini, M., Souto, E. B., and Santini, A. Characteristics, occurrence, detection and detoxification of aflatoxins in foods and feeds. *Foods*, 9(5):644, 2020.

[17] Papillomaviruses, H. IARC monographs on the evaluation of carcinogenic risks to humans. *Lyon, France, IARC,* 2011.

[18] Radhapyari, K., and Khan, R. Amperometric immuno-sensor for detection of toxin aflatoxin B_1 based on polyaniline probe modified with Mc-IgGs-a-AFB_1 antibodies. *Advanced Materials Letters,* 5(8):435-440, 2014.

[19] Zhu, C., Yang, G., Li, H., Du, D., and Lin, Y. Electrochemical sensors and biosensors based on nanomaterials and nanostructures. *Analytical chemistry*, 87(1):230-249, 2015.

[20] Sun, A. C., Yao, C., Venkatesh, A. G., and Hall, D. A. An efficient power harvesting mobile phone-based electrochemical biosensor for point-of-care health monitoring. *Sensors and Actuators B: chemical*, 235:126-135, 2016.

[21] Mishra, S., and Deshmukh, R. Overview of advancement in biosensing technology, including its applications in healthcare. *Current Pharmaceutical Biotechnology*, 24(3):411-426, 2023.

[22] Aydemir, N., Malmström, J., and Travas-Sejdic, J. Conducting polymer based electrochemical biosensors. *Physical Chemistry Chemical Physics*, 18(12):8264-8277, 2016.

[23] Liu, Y., Turner, A. P., Zhao, M., and Mak, W. C. Processable enzyme-hybrid conductive polymer composites for electrochemical biosensing. *Biosensors and Bioelectronics*, 100:374-381, 2018.

[24] Tan, E., Pappa, A. M., Pitsalidis, C., Nightingale, J., Wood, S., Castro, F. A., ... and Kim, J. S. A highly sensitive molecular structural probe applied to in situ biosensing of metabolites using PEDOT: PSS. *Biotechnology and Bioengineering*, 117(1):291-299, 2020.

[25] Luo, X., Weaver, C. L., Tan, S., and Cui, X. T. Pure graphene oxide doped conducting polymer nanocomposite for bio-interfacing. *Journal of Materials Chemistry B*, 1(9):1340-1348, 2013.

[26] Xu, J., Wang, Y., and Hu, S. Nanocomposites of graphene and graphene oxides: synthesis, molecular functionalization and application in electrochemical sensors and biosensors. A review. *Microchimica Acta*, 184:1-44, 2017.

[27] Thangamuthu, M., Hsieh, K. Y., Kumar, P. V., and Chen, G. Y. Graphene-and graphene oxide-based nanocomposite platforms for electrochemical biosensing applications. *International journal of molecular sciences*, 20(12):2975, 2019.

[28] Jazayeri, M. H., Amani, H., Pourfatollah, A. A., Pazoki-Toroudi, H., and Sedighimoghaddam, B. Various methods of gold nanoparticles (GNPs) conjugation to antibodies. *Sensing and bio-sensing research*, 9:17-22, 2016.

[29] Gligor, D., Cuibus, F., Peipmann, R., and Bund, A. Novel amperometric sensors for nitrite detection using electrodes modified with PEDOT prepared in ionic liquids. *Journal of Solid State Electrochemistry*, 21:281-290, 2017.

[30] Sharma, A., Kumar, A., and Khan, R. A highly sensitive amperometric immunosensor probe based on gold nanoparticle functionalized poly (3, 4-ethylenedioxythiophene) doped with graphene oxide for efficient detection of aflatoxin B_1. *Synthetic Metals*, 235:136-144, 2018.

[31] Chi, Q., Zhang, J., Dong, S., and Wang, E. Direct electrochemistry and surface characterization of glucose oxidase adsorbed on anodized carbon electrodes. *Electrochimica Acta*, 39(16):2431-2438, 1994.

[32] Christwardana, M., Chung, Y., and Kwon, Y. A correlation of results measured by cyclic voltammogram and impedance spectroscopy in glucose oxidase based biocatalysts. *Korean Journal of Chemical Engineering*, 34:3009-3016, 2017.

[33] Zhang, X., Liu, D., Li, L., and You, T. Direct electrochemistry of glucose oxidase on novel free-standing nitrogen-doped carbon nanospheres@ carbon nanofibers composite film. *Scientific reports*, 5(1):9885, 2015.

[34] Cai, C., and Chen, J. Direct electron transfer of glucose oxidase promoted by carbon nanotubes. *Analytical biochemistry*, 332(1):75-83, 2004.

[35] Liang, W., and Zhuobin, Y. Direct electrochemistry of glucose oxidase at a gold electrode modified with single-wall carbon nanotubes. *Sensors*, 3(12):544-554, 2003.

[36] Shrivastava, A., and Gupta, V. B. Methods for the determination of limit of detection and limit of quantitation of the analytical methods. *Chronicles of Young Scientists*, 2(1):21-25, 2011.

[37] Thakur, B., Amarnath, C. A., and Sawant, S. N. Pectin coated polyaniline nanoparticles for an amperometric glucose biosensor. *RSC advances*, 4(77):40917-40923, 2014.

[38] German, N., Ramanaviciene, A., and Ramanavicius, A. Dispersed conducting polymer nanocomposites with glucose oxidase and gold nanoparticles for the design of enzymatic glucose biosensors. *Polymers*, 13(13):2173, 2021.

[39] Tang, W., Li, L., and Zeng, X. A glucose biosensor based on the synergistic action of nanometer-sized TiO_2 and polyaniline. *Talanta*, 131:417-423, 2015.

[40] Shrestha, B. K., Ahmad, R., Mousa, H. M., Kim, I. G., Kim, J. I., Neupane, M. P., ... and Kim, C. S. High-performance glucose biosensor based on chitosan-glucose oxidase immobilized polypyrrole/Nafion/functionalized multi-walled carbon nanotubes bio-nanohybrid film. *Journal of colloid and interface science*, 482:39-47, 2016.

[41] Maity, D., Minitha, C. R., and RT, R. K. Glucose oxidase immobilized amine terminated multiwall carbon nanotubes/reduced graphene oxide/polyaniline/gold nanoparticles modified screen-printed carbon electrode for highly sensitive amperometric glucose detection. *Materials Science and Engineering: C*, 105:110075, 2019.

[42] Kadian, S., Arya, B. D., Kumar, S., Sharma, S. N., Chauhan, R. P., Srivastava, A., ... and Singh, S. P. Synthesis and application of PHT-TiO_2 nanohybrid for amperometric glucose detection in human saliva sample. *Electroanalysis*, 30(11):2793-2802, 2018.

[43] Betty, C. A., Lal, R., Yakhmi, J. V., and Kulshreshtha, S. K. Time response and stability of porous silicon capacitive immunosensors. *Biosensors and Bioelectronics*, 22(6):1027-1033, 2007.

[44] Betty, C. A. Highly sensitive capacitive immunosensor based on porous silicon–polyaniline structure: Bias dependence on specificity. *Biosensors and Bioelectronics*, 25(2):338-343, 2009.

[45] Medhi, A., Baruah, S., Singh, J., Betty, C. A., and Mohanta, D. Au nanoparticle modified GO/PEDOT-PSS based immunosensor probes for sensitive and selective detection of serum immunoglobulin g (IgG). *Applied Surface Science*, 575:151775, 2022.

[46] Sharma, A., Kumar, A., and Khan, R. Electrochemical immunosensor based on poly (3, 4-ethylenedioxythiophene) modified with gold nanoparticle to detect aflatoxin B_1. *Materials Science and Engineering: C*, 76:802-809, 2017.

[47] Bhardwaj, H., Pandey, M. K., Rajesh, and Sumana, G. Electrochemical Aflatoxin B_1 immunosensor based on the use of graphene quantum dots and gold nanoparticles. *Microchimica Acta*, 186:1-12, 2019.

[48] Park, J. H., Kim, Y. P., Kim, I. H., and Ko, S. Rapid detection of aflatoxin B_1 by a bifunctional protein crosslinker-based surface plasmon resonance biosensor. *Food Control*, 36(1):183-190, 2014.

[49] Althagafi, I. I., Ahmed, S. A., and El-Said, W. A. Colorimetric aflatoxins immunoassay by using silica nanoparticles decorated with gold nanoparticles. *Spectrochimica Acta Part A: Molecular and Biomolecular Spectroscopy*, 246:118999, 2021.

[50] Gualandi, I., Tonelli, D., Mariani, F., Scavetta, E., Marzocchi, M., and Fraboni, B. Selective detection of dopamine with an all PEDOT: PSS organic electrochemical transistor. *Scientific reports*, 6(1):35419, 2016.

[51] Shakeel, Q., Lyu, A., Zhang, J., Wu, M., Li, G., Hsiang, T., and Yang, L. Biocontrol of Aspergillus flavus on peanut kernels using Streptomyces yanglinensis 3-10. *Frontiers in microbiology*, 9:1049, 2018.

[52] Kamal, A. S. M., Khair, A., Dawlatana, M., Hassan, M. T., Begum, F., and Rahim, M. Evaluation of aflatoxins and pesticide residues in fresh and different processed mushrooms. *Bangladesh Journal of Scientific and Industrial Research*, 44(2):193-198, 2009.